Cell

Roquin Promotes Constitutive mRNA Decay via a Conserved Class of Stem-Loop Recognition Motifs

Kathrin Leppek,[1] Johanna Schott,[1] Sonja Reitter,[1] Fabian Poetz,[1] Ming C. Hammond,[2] and Georg Stoecklin[1,*]
[1]Helmholtz Junior Research Group Posttranscriptional Control of Gene Expression, German Cancer Research Center, DKFZ-ZMBH Alliance, Im Neuenheimer Feld 280, 69120 Heidelberg, Germany
[2]Department of Chemistry and Department of Molecular and Cell Biology, University of California, Berkeley, Berkeley, CA 94720, USA
*Correspondence: g.stoecklin@dkfz.de
http://dx.doi.org/10.1016/j.cell.2013.04.016

SUMMARY

Tumor necrosis factor-α (TNF-α) is the most potent proinflammatory cytokine in mammals. The degradation of TNF-α mRNA is critical for restricting TNF-α synthesis and involves a constitutive decay element (CDE) in the 3′ UTR of the mRNA. Here, we demonstrate that the CDE folds into an RNA stem-loop motif that is specifically recognized by Roquin and Roquin2. Binding of Roquin initiates degradation of TNF-α mRNA and limits TNF-α production in macrophages. Roquin proteins promote mRNA degradation by recruiting the Ccr4-Caf1-Not deadenylase complex. CDE sequences are highly conserved and are found in more than 50 vertebrate mRNAs, many of which encode regulators of development and inflammation. In macrophages, CDE-containing mRNAs were identified as the primary targets of Roquin on a transcriptome-wide scale. Thus, Roquin proteins act broadly as mediators of mRNA deadenylation by recognizing a conserved class of stem-loop RNA degradation motifs.

INTRODUCTION

The ability of cells to rapidly alter their gene expression program is dependent on both transcriptional and posttranscriptional mechanisms. The lifespan of messenger RNAs (mRNAs) is increasingly recognized as an important determinant of gene expression levels. Short half-lives are particularly important for dynamically regulated transcripts whose expression needs to be turned on and off rapidly. This includes mRNAs encoding transcription factors, signaling components, cell cycle proteins, and regulators of immune responses (Hao and Baltimore, 2009; Rabani et al., 2011; Schwanhäusser et al., 2011).

Many elements that destabilize mRNAs are recognized by *trans*-acting factors as linear sequences. In eukaryotes, a prominent example is the AU-rich element (ARE), a divergent and potent class of destabilizing sequences that is located in the 3′ UTR and controls the degradation of many cytokine and transcription factor mRNAs (Garneau et al., 2007). Likewise, microRNA (miRNA)-binding sites are recognized as linear sequences; imperfect base-pairing with miRNAs leads to recruitment of argonaute and TNRC6 proteins, which, in turn, cause translation repression or mRNA degradation (Huntzinger and Izaurralde, 2011).

Few examples also exist for structured RNA degradation motifs. In histone mRNAs, a highly conserved stem-loop at the end of the 3′ UTR is recognized by the stem-loop binding protein (SLBP), which mediates rapid mRNA degradation at the end of S phase (Marzluff et al., 2008). Interleukin (IL)-6 mRNA is degraded directly through a stem-loop within its 3′ UTR that is recognized by the endonuclease Zc3h12a (Matsushita et al., 2009). Beyond these individual examples, computational approaches suggest that structured mRNA motifs are more abundant and form distinct families (Goodarzi et al., 2012; Parker et al., 2011).

A prominent example for extensive posttranscriptional control is tumor necrosis factor-α (TNF-α), the most potent proinflammatory cytokine in mammals (Tracey and Cerami, 1994). The local production of TNF-α at sites of injury or infection is important to trigger an immune response, yet its systemic or chronic release has detrimental consequences by causing septic shock and chronic inflammatory diseases (Bradley, 2008). Tight posttranscriptional control of TNF-α expression requires several regulatory elements in the 3′ UTR. An ARE suppresses translation and causes rapid mRNA degradation in the cytoplasm. It is recognized by ARE-binding proteins such as TTP, a zinc finger (ZF) protein that promotes rapid mRNA decay (Carballo et al., 1998) by recruiting the Ccr4-Caf1-Not deadenylase complex (Sandler et al., 2011), the decapping enzyme Dcp2 (Fenger-Grøn et al., 2005), and the exosome (Chen et al., 2001). Besides the ARE, miRNA miR-125b participates in dampening TNF-α expression (Androulidaki et al., 2009). In addition, we previously described the constitutive decay element (CDE) as a destabilizing activity in the TNF-α 3′ UTR (Stoecklin et al., 2003). Whereas ARE-mediated mRNA decay is transiently blocked during macrophage stimulation, the CDE was found to cause constitutive mRNA decay, thereby limiting the expression of this potentially harmful cytokine under proinflammatory conditions.

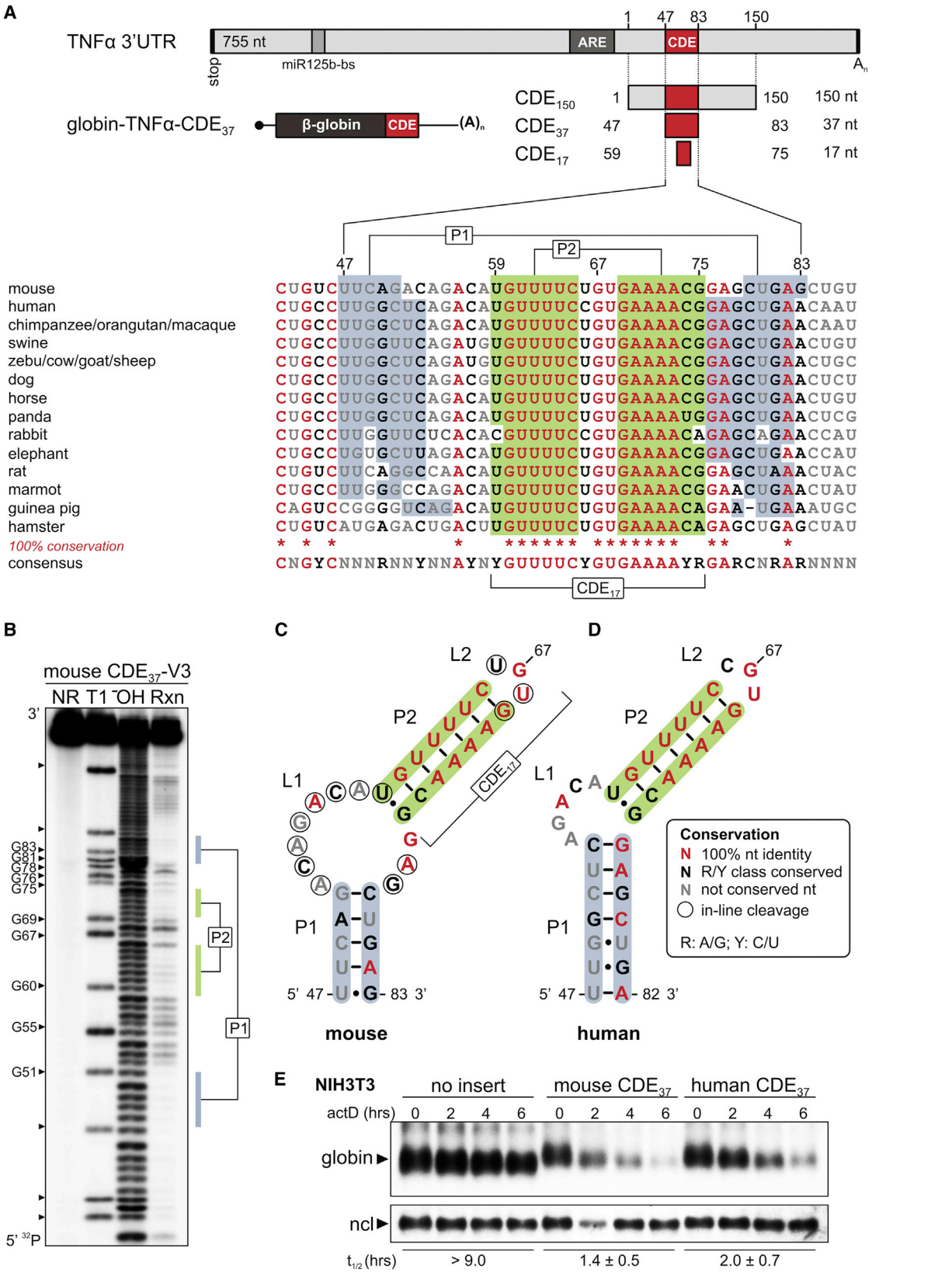

(legend on next page)

Here, we report that the CDE is a structured motif that folds into an RNA stem-loop in its active conformation. We purified Roquin and Roquin2 as stem-loop-specific CDE-binding proteins, and demonstrate that Roquin is required for CDE-mediated mRNA decay and suppression of TNF-α production in macrophages. We further show that Roquin proteins cause mRNA deadenylation by recruiting the Ccr4-Caf1-Not complex. Finally, we discovered target mRNAs of Roquin on a transcriptome-wide scale and provide evidence that Roquin controls the degradation of numerous mRNAs with conserved CDE stem-loop motifs.

RESULTS

The CDE Is a Conserved Stem-Loop Motif

Previously, the CDE had been mapped to an 80-nucleotide (nt)-long sequence in the mouse TNF-α 3′ UTR (Stoecklin et al., 2003). Decay assays with globin-TNF-α reporter mRNAs in transiently transfected NIH 3T3 cells (Figure S1A available online) allowed us to narrow down the element to a 37-nt-long fragment (CDE_{37}; Figure 1A; Figure S1B). As CDE mRNA decay was not affected by knockout of Dicer (Figures S1C–S1E), the CDE is unlikely to serve as a miRNA binding site. The decay activity of CDE_{37} was strongly influenced by the context into which it was cloned (compare versions V2 and V3 in Figures S2A and S2B; Table S1), suggesting that the CDE might be a structured element. To address its structure experimentally, we applied in-line probing, an RNA cleavage assay in which base-paired or structurally constrained nucleotides are protected from spontaneous phosphodiester bond hydrolysis. The cleavage reaction (Figure 1B) revealed that the highly active CDE_{37}-V3 folds into a P2-L2 stem-loop, which is flanked by an internal L1 loop followed by a P1 stem (Figure 1C). Regions protected from cleavage precisely correspond to the base-paired regions of the P1 and P2 stems, whereas cleavage sites (circled in Figure 1C) were observed at most nucleotides in the L1 and L2 loops. In contrast, the less active CDE_{37}-V2 showed a diffuse cleavage pattern that could not be assigned to a predominant structure (Figure S2C). In-line probing of a 150-nt-long RNA containing the CDE in its native context (CDE_{150}) also resulted in a diffuse cleavage pattern (Figure S2C). Like CDE_{37}-V2, CDE_{150} was less active in mediating mRNA decay than CDE_{37}-V3 (Figure S2B). The stem-loop structures in both CDE_{37}-V2 and CDE_{150} also provide a much smaller decrease in free energy as compared to CDE_{37}-V3 (Figure S2A). This indicated that the highly active CDE_{37}-V3 adopts a stable structure, whereas the less active CDE_{37}-V2 and CDE_{150} appear to fluctuate between alternative or unstructured conformations.

It is important to note that the human CDE sequence can fold into a similar P1-L1-P2-L2 structure (Figure 1D) and, like the mouse CDE, causes rapid mRNA degradation (Figure 1E). Comparison of TNF-α CDE sequences from 19 mammalian species showed that the P2-L2 stem-loop is conserved to nearly 100%, whereas the P1 and L1 sequences are more divergent (Figure 1A). Sequence substitution analysis revealed that mutations within the P1 stem or the L1 loop did not affect CDE mRNA decay (Figures S3A–S3C). In contrast, all mutations disrupting P2 or L2 inactivated the CDE, pointing toward the importance of the highly conserved P2-L2 stem-loop.

The P2-L2 Stem-Loop Is Sufficient for CDE-Mediated mRNA Decay

We then tested by mutagenesis whether the CDE's ability to fold into a stem-loop is required for mRNA decay. All mutations disrupting the P2 stem (M16, M19, M21, and M22) abrogated CDE_{37} activity (Figure 2A; Figure S3D). Whereas compensatory mutations restoring the apical part of P2 remained inactive (M23 and M27), compensatory mutations in the basal part of the stem rescued CDE_{37} activity (M20 and M26; Figure S3D). It is important to note that the compensatory mutation M20 was also able to restore activity of CDE_{150} (Figure 2B), demonstrating the existence of a functional P2 stem in the context of the native TNF-α 3′ UTR. Taken together, both stem structure and nt identity in the apical 3 base pairs of P2 are essential for CDE activity, whereas base-pairing alone is sufficient in the basal part of P2.

Analysis of the trinucleotide L2 loop revealed that changing its middle position (nt 67) from G to A did not abrogate CDE_{37} activity (M24; Figure 2C). Variation is also tolerated at position 66, where the human CDE has a C as opposed to a U in the mouse L2 loop (Figures 1C–1E). However, decay activity was lost when the entire UGU loop was replaced by ACA (M25; Figure 2C), indicating that the CDE allows only for limited nt variation in the L2 loop.

It is interesting that the P2-L2 stem-loop alone was sufficient to promote rapid mRNA degradation when an open, single-stranded (ss) conformation was provided at the base of the P2 stem (CDE_{17}-ss; Figure 2D). In contrast, the CDE was inactive when the P2 stem was elongated (CDE_{17}-ds [double stranded]), suggesting that the L1 loop at the base of P2 is also an important structural feature of the CDE. From these experiments, we

Figure 1. The Active TNF-α CDE Is a Conserved RNA Stem-Loop Motif

(A) Schematic representation of the mouse TNF-α 3′ UTR together with an alignment of 19 mammalian TNF-α CDE sequences. The nts are color coded according to conservation as indicated in (D); R, purine; Y, pyrimidine. Numbers refer to nt positions within the CDE_{150} fragment.

(B) In-line probing analysis of in vitro synthesized, 5′-labeled CDE_{37}-V3 RNA. V3 refers to a cloning context permissive to CDE activity. The RNA was loaded directly (NR, no reaction), subjected to cleavage by RNase T1 or alkaline hydrolysis ($^{-}$OH), or incubated for 45 hr at room temperature and pH 8.3 (in-line reaction, Rxn) prior to urea-PAGE.

(C) Secondary structure model of the mouse TNF-α CDE_{37} RNA derived from in-line probing. The nts 5′ to cleavage sites are circled; pairing elements P1 and P2 are shaded in blue and green, respectively; and nts are color coded according to conservation. Mfold calculation of $\Delta G = -6.7$ kcal/mol for CDE_{37} as depicted, $\Delta G = -18.7$ kcal/mol for CDE_{37}-V3.

(D) Secondary structure model predicted for the human TNF-α CDE_{37} RNA by thermodynamic modeling; $\Delta G = -9.0$ kcal/mol.

(E) Globin reporter genes containing no insert in the 3′ UTR, mouse CDE_{37}-V3, or human CDE_{37}-V3 were transiently transfected into NIH 3T3 cells. Upon treatment with actinomycin D (actD), total RNA was extracted at 2 hr intervals, resolved on 1.1% agarose gels, and subjected to northern blot analysis. Globin mRNA signals normalized to nucleolin (ncl) were used for calculation of average mRNA half-lives ($t_{1/2}$) ± SD, $n \geq 3$.

See also Figures S1, S2, and S3 and Table S1.

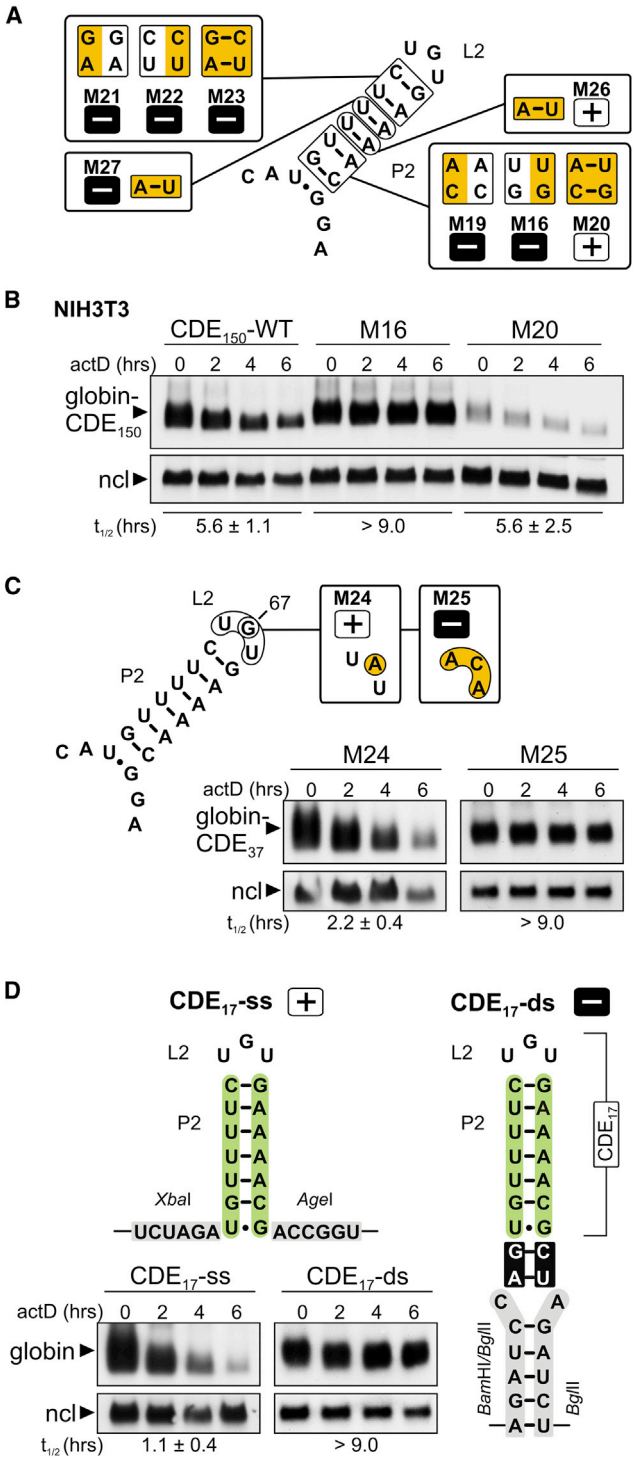

Figure 2. Mutational Analysis of the TNF-α CDE Stem-Loop

(A) P2 stem mutations were introduced into the TNF-α CDE, either in one strand to disrupt P2 or as compensatory mutations to restore P2. The mutated CDE_{37} fragments were cloned in the V3 context into the 3′ UTR of the globin reporter gene, and mRNA decay was measured in transiently transfected NIH 3T3 cells, average $t_{1/2}$ ± SD, n ≥ 3. CDE mutants active in mRNA decay ($t_{1/2}$ < 6.0 hr) are labeled "+," and inactive mutants ($t_{1/2}$ > 9.0 hr) are labeled "−." Northern blots are depicted in Figure S3D.

concluded that the 17-nt-long P2-L2 stem-loop with unpaired flanking nts is the minimal element sufficient to induce CDE-mediated mRNA decay.

Roquin and Roquin2 Bind to the CDE

With the aim to identify CDE-interacting proteins, we developed 4xS1m, an RNA aptamer with higher binding efficiency to streptavidin as compared to the previously described S1 aptamer (Srisawat and Engelke, 2001). Of note, 4xS1m alone does not induce mRNA decay, nor does it interfere with CDE mRNA decay (Figure S4A). In vitro transcribed CDE_{37}-4xS1m and control 4xS1m RNAs were coupled to streptavidin for affinity purification of proteins from NIH 3T3 cell lysates (Figure S4B). Although most purified proteins were associated with both RNAs, we were able to identify proteins specifically enriched with CDE_{37}-4xS1m by mass spectrometry (Table S2). Strongest peptide enrichment was observed for Roquin (i.e., Rc3h1, RING finger and CCCH zinc finger protein 1). Its paralog Rc3h2, which we refer to as Roquin2, was also purified specifically with CDE_{37}-4xS1m. Roquin has previously been described as a protein that prevents autoimmunity by destabilizing the mRNA that encodes inducible T cell costimulator (ICOS) (Yu et al., 2007).

By RNA immunoprecipitation (IP), we verified that enhanced green fluorescent protein (EGFP)-Roquin and -Roquin2 strongly associate with globin-CDE_{150}, but not with the globin mRNA alone (Figure 3A). Disrupting the P2 stem in the CDE mutant M16 dramatically reduced binding to EGFP-Roquin, while restoring the stem through a compensatory mutation in M20 rescued Roquin-binding (Figure 3A). Thus, Roquin recognizes the CDE as a stem-loop motif.

We then tested, by in vivo crosslinking, whether the Roquin-CDE association occurs inside cells and not postlysis. Figure 3B shows that, in the absence of formaldehyde crosslinking, EGFP-Roquin associates with globin-CDE_{37} mRNA under nondenaturing conditions (lane 3), but not under denaturing conditions (4 M urea, lane 4). When cells were crosslinked prior to lysis, globin-CDE_{37} mRNA remained associated with EGFP-Roquin under denaturing conditions (lanes 5 and 6). Because EGFP-Roquin does not bind globin mRNA lacking a CDE under either condition (Figure S4C), these experiments demonstrate specific association of Roquin with CDE mRNA inside cells.

Roquin contains a RING finger, a ROQ domain, a ZF, and a poorly defined C-terminal, proline-rich domain (Figure 3C). Although ZFs are frequently involved in RNA binding, mutation of the ZF in Roquin (C419R, Figure S4D) did not affect its association with globin-CDE_{37} mRNA (Figure S4E). Whereas

(B) P2 disrupting mutation M16 and compensatory mutation M20 were introduced into globin-TNF-α-CDE_{150}, and mRNA decay was measured in transiently transfected NIH 3T3 cells by northern blot analysis, average $t_{1/2}$ ± SD, n ≥ 3.

(C) L2 loop mutations were introduced into globin-TNF-α-CDE_{37}-V3, and corresponding mRNA half-lives (average $t_{1/2}$ ± SD, n = 4) were measured as in (B).

(D) The 17-nt-long TNF-α P2-L2 stem-loop (CDE_{17}) was tested in two different cloning contexts that provide a single-stranded (ss) or double-stranded (ds) conformation at the base of P2. Reporter mRNA half-lives (average $t_{1/2}$ ± SD, n = 3) were measured as in (B).

See also Figure S3 and Table S1.

deletion of the RING domain (ΔRING) had no effect either, deletion of the ROQ domain (ΔROQ) prevented binding to the CDE_{37} reporter mRNA (Figure 3D). In line with this result, Roquin N-term, as well as the ROQ domain alone, was able to associate with globin-CDE_{37} mRNA, whereas Roquin C-term was not (Figure 3E).

By electromobility shift assay (EMSA), we then examined whether Roquin interacts directly with the CDE RNA in vitro. Recombinant Roquin-N (amino acids 2–440; Figure S4F) (Glasmacher et al., 2010) was found to bind efficiently to a 23-nt-long CDE stem-loop RNA (CDE_{23}) with an apparent dissociation constant (K_d) of 92 nM (Figure 3F). In contrast, the mutant CDE_{23}-M23 harboring a compensatory 2 base pair mutation in the functionally important apical part of P2 did not associate with Roquin-N, and an unstructured ARE RNA of identical length did not bind either (Figure 3F). From these experiments, we concluded that Roquin recognizes the CDE stem-loop with high specificity both in vitro and inside cells.

Roquin and Roquin2 Promote CDE-Mediated mRNA Decay

As a first test for Roquin function, ectopically expressed EGFP-Roquin or -Roquin2 (Figure S4G) were found to accelerate degradation of globin-CDE_{150} and globin-CDE_{37} mRNAs in both NIH 3T3 and HeLa cells, whereas the reporter mRNA lacking a CDE was not affected by Roquin overexpression (Figure 4A; Figures S4H–S4J).

Taking the opposite approach, we then examined the effect of knocking down Roquin and Roquin2. In NIH 3T3 cells, knockdown (kd) of either protein alone (Figure S5A) caused a modest 2-fold stabilization of globin-CDE_{37} mRNA, whereas the simultaneous kd of both proteins led to a 7-fold stabilization (Figures 4B and S5B). Expression of a small interfering RNA (siRNA)-resistant Roquin cDNA (Figure S5C) restored degradation of the CDE_{37} reporter mRNA after kd of endogenous Roquin/Roquin2 (Figure 4C), demonstrating specificity of Roquin kd.

These results were corroborated in lipopolysaccharide (LPS)-stimulated RAW264.7 macrophages, where kd of Roquin by two different siRNAs (Figure 4D) led to a 2- to 4-fold stabilization of endogenous TNF-α mRNA (Figure 4E). Of note, Roquin kd prevented rapid clearance of TNF-α mRNA during prolonged exposure of macrophages to LPS (Figure 4F) and caused elevated levels of both membrane-bound and secreted TNF-α as shown by western blot analysis and ELISA (Figures 4G and 4H). The simultaneous kd of Roquin and Roquin2 did not cause a further increase in TNF-α mRNA (Figure S5D) or protein (Figure S5E) levels as compared to kd of Roquin alone, presumably because Roquin depletion was less efficient in the double-kd condition (Figure S5F). In unstimulated macrophages, TNF-α mRNA was also stabilized upon kd of Roquin (Figure 4I). Taken together, these results demonstrate that Roquin, by binding to the CDE and accelerating mRNA decay, is crucial for limiting TNF-α production in both resting and activated macrophages.

Roquin Promotes mRNA Deadenylation by Recruitment of the Ccr4-Caf1-Not Complex

To further explore the mechanism of Roquin-induced mRNA decay, EGFP, EGFP-Roquin, and EGFP-Roquin2 were stably expressed in HEK293 cells and affinity purified. Mass spectrometry revealed Not1 to be strongly associated with both Roquin and Roquin2 (Table S3). Not1 is the scaffold subunit of the Ccr4-Caf1-Not complex, a major deadenylase in eukaryotic cells (Collart and Panasenko, 2012). Indeed, virtually all the other subunits of the complex, including Not2, Not3, Not10, TAB182, Ccr4b, Caf1a, and Caf1b, were also enriched in the Roquin and Roquin2 purifications (Table S3). By coimmunoprecipitation (co-IP), we confirmed that EGFP-Roquin and -Roquin2 interact with endogenous Not1 and Caf1a in an RNA-independent manner (Figure 5A). Residual binding of Caf1a to the negative control, EGFP, was observed in some (Figure 5A), but not all, experiments (Figure S6A).

We then tested Caf1a-AA, a dominant-negative mutant of the deadenylase Caf1a (Sandler et al., 2011), and found that its overexpression fully blocked both deadenylation and degradation of globin-CDE_{37} mRNA (Figure 5B). As opposed to Caf1a-AA, neither Caf1a-WT (Figure S6B) nor the dominant-negative decapping enzyme Dcp2-AA (Figure 5B) affected CDE mRNA decay. These data provide strong evidence that Roquin recruits the Ccr4-Caf1-Not complex and thereby induces rapid deadenylation and subsequent degradation of its target mRNAs.

While the ROQ domain within the N terminus of Roquin binds to the CDE RNA (Figures 3D–3F), we found that the C-terminal domain associates with Not1 and Caf1a (Figure 5C). As expected, the RNA-binding-deficient Roquin-ΔROQ mutant was unable to accelerate degradation of globin-CDE_{37} mRNA (Figure S6C). In comparison to EGFP alone, expression of the individual N-terminal, C-terminal, and ROQ domains (Figure S6D) stabilized globin-CDE_{37} mRNA (Figure 5D), suggesting that Roquin fragments have dominant-negative activity. This could be explained by a competition of endogenous Roquin with the N-terminal ROQ domain for CDE mRNA binding. Likewise, endogenous Roquin may compete with the C-terminal Roquin fragment for Ccr4-Caf1-Not complex binding.

Roquin Recognizes a Conserved Class of CDE-Containing mRNAs

Roquin was reported to enhance the degradation of ICOS mRNA (Yu et al., 2007), yet the exact binding motif was unknown. By inspecting the ICOS sequence, we found a highly conserved CDE-like element in the ICOS 3′ UTRs (Figures S7A and S7B). Although the stem in the ICOS element is 2 base pairs shorter than the P2 stem in the TNF-α CDE, the functionally important apical part of the stem is identical in sequence. When cloned into the ss globin 3′ UTR context, ICOS CDE_{17}-ss induced reporter mRNA decay, which was further accelerated by overexpression of EGFP-Roquin (Figure S7C). These results imply that Roquin recognizes the ICOS mRNA via a CDE-like stem-loop motif.

With the aim to predict CDE-containing mRNAs genome-wide, we derived a structure- and sequence-based CDE consensus motif from our experimental data (Figure 6A). By searching all 3′ UTRs of the mouse transcriptome, we identified 109 putative CDEs in 108 genes (Table S4). Notably, 56 of the identified CDEs are highly conserved in more than 10 of 46 vertebrate species (Figure 6B; yellow in Table S4), and the corresponding genes are preferentially associated with regulation of development, transcription, nucleic acid metabolism, and T cell differentiation (Table S5).

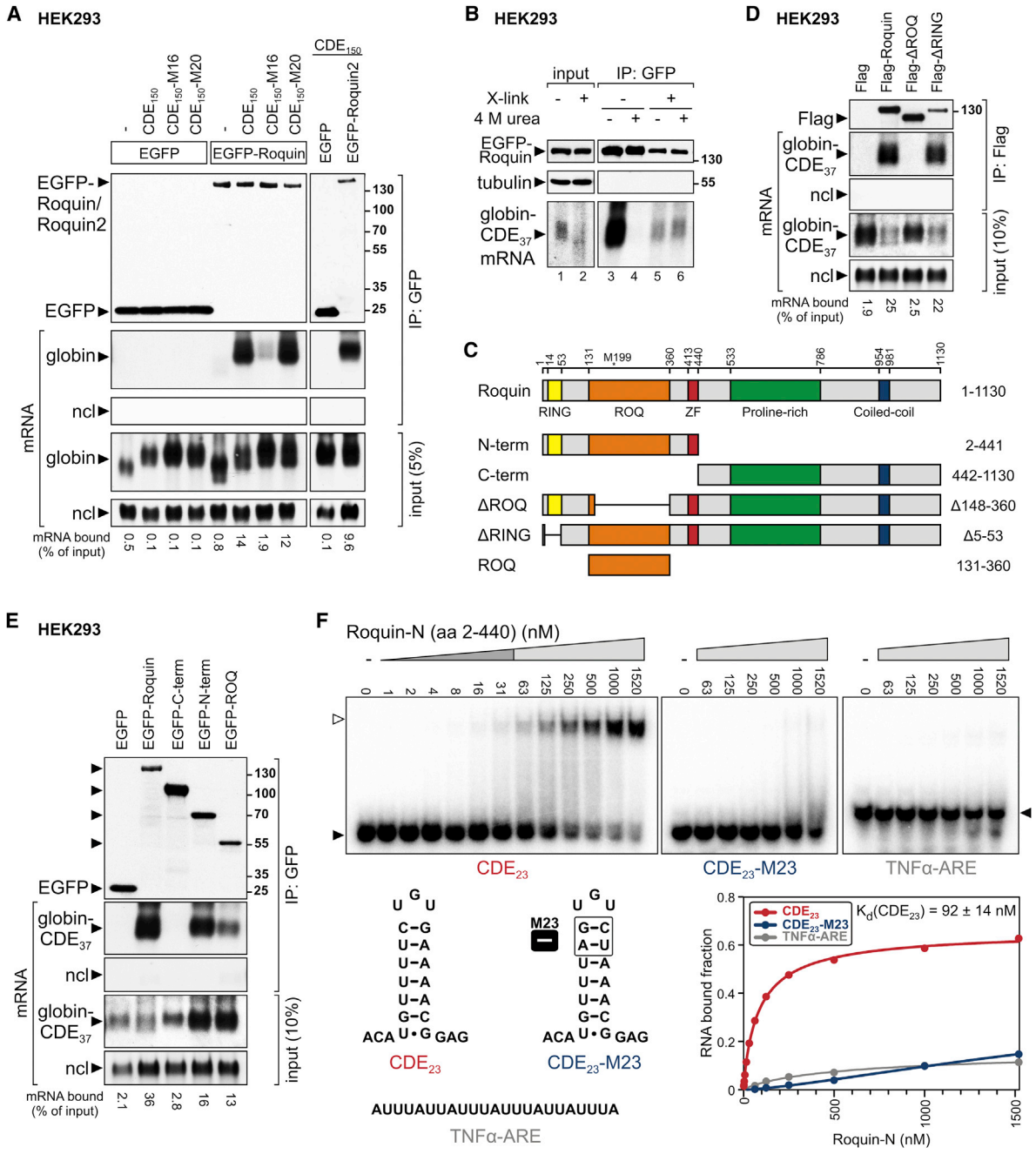

Figure 3. Specific Binding of Roquin to the CDE In Vitro and Inside Cells

(A) Binding of Roquin to the mouse TNF-α CDE_{150} was analyzed by RNA IP. HEK293 cells were transiently transfected with EGFP, EGFP-Roquin, or -Roquin2 together with a globin reporter lacking an insert (–), globin-TNF-α-CDE_{150}, or the corresponding M16 and M20 mutants. After IP, EGFP-tagged proteins were monitored by anti-GFP western blot analysis. Associated reporter mRNAs were visualized by northern blot analysis; ncl mRNA serves as negative control. The fraction of mRNA bound by IP is given as the percentage of input.

(B) Binding of Roquin to the globin-TNF-α-CDE_{37} mRNA was analyzed by RNA IP after crosslinking. HEK293 cells were transiently transfected with EGFP-Roquin together with globin-TNF-α-CDE_{37}-V3. Where indicated (X-link), cells were treated with 0.05% formaldehyde before lysis. EGFP-Roquin was immunoprecipitated either under nondenaturing conditions or under denaturing conditions (4 M urea). See also Figure S4C.

(C) Schematic representation of mouse Roquin domains. Deletion mutants are depicted below the full-length protein. Numbers indicate amino acid positions, M199 refers to the position mutated in *sanroque* mice.

(D) HEK293 cells were transiently transfected with globin-TNF-α-CDE_{37}-V3 together with Flag vector alone, Flag-Roquin, Flag-Roquin-ΔROQ or Flag-Roquin-ΔRING. After Flag IP, reporter mRNA binding was monitored as in (A).

(E) HEK293 cells were transiently transfected with globin-TNF-α-CDE_{37}-V3 together with EGFP, EGFP-tagged Roquin, C-term, N-term, or ROQ. After EGFP IP, reporter mRNA binding was monitored as in (A).

(legend continued on next page)

To determine Roquin target mRNAs experimentally, we immunoprecipitated endogenous Roquin from cytoplasmic lysates of LPS-stimulated macrophages (Figure S7D) and identified Roquin-associated mRNAs (Table S6) by deep sequencing of RNA samples from three biological replicates (Figure S7E). Remarkably, mRNAs with conserved CDEs in the 3′ UTR showed a strong and highly significant enrichment in the Roquin IP (red in Figure 6C; frequency of association in Figure 6B). The top Roquin target (475-fold enrichment) was Nfkbid mRNA, which also represents the only mouse transcript that contains a tandem CDE stem-loop motif in its 3′ UTR (Figure 6D). The mRNAs encoding Roquin and Roquin2 themselves contain conserved CDEs and were enriched by Roquin IP, suggesting that Roquin proteins may regulate their own mRNAs as part of a feedback loop. Consistent with our previous results, TNF-α and ICOS mRNA were strongly enriched by Roquin IP. Thus, an unbiased RNA IP approach provided compelling evidence that CDE-containing mRNAs are the primary targets of Roquin.

We then verified binding of several mRNAs containing conserved CDEs (Figures 6D and S7F) by IP of endogenous Roquin followed by RT-qPCR. TNF-α mRNA was found to associate with Roquin to a similar degree in resting and stimulated macrophages (Figure 6E, left). In contrast to four control mRNAs lacking a CDE, six of seven mRNAs with conserved CDEs were strongly enriched ($\geq$20-fold) by Roquin IP from LPS-stimulated RAW264.7 macrophages (Figure 6E, right).

We further investigated whether Roquin controls the degradation of newly identified, CDE-containing target mRNAs. Indeed, kd of Roquin and Roquin2 led to the stabilization of Nfkbiz, Ier3, Ppp1r10 and Hmgxb3 mRNA in NIH 3T3 cells, and ectopic expression of siRNA-resistant Roquin restored the degradation of these mRNAs (Figure 6F). Nfkbid mRNA could not be analyzed in NIH 3T3 cells due to its low expression level but was found to be stabilized by kd of Roquin in RAW264.7 macrophages (Figure S7G). These results demonstrate that Roquin regulates the degradation of numerous mRNAs containing CDE stem-loop motifs.

Interference with CDE-Roquin Binding Alleviates TNF-α Suppression

Finally, we explored whether Roquin-mediated mRNA regulation could be blocked with a *trans*-acting antisense morpholino (MO) that interferes with CDE stem-loop formation. CDE-MO-1 and -2 were designed to base pair with the left and right arms of the TNF-α CDE stem-loop, respectively (Figure 7A). As controls, we used Ctrl-MO lacking any target sequence and UTR-MO, a MO that base-pairs with the TNF-α 3′ UTR downstream of the CDE. RNA IP showed that CDE-MO-2 reduces binding of Roquin to the 3′ UTR of TNF-α mRNA by 4-fold (Figure 7B). In contrast, CDE-MO-1 was not able to compete with CDE-Roquin binding, presumably because the portion that needs to invade the P2-L2 stem-loop is shorter in CDE-MO-1 (7 nt) than in CDE-MO-2 (11 nt). When introduced into RAW264.7 macrophages, CDE-MO-2 specifically increased the expression of endogenous TNF-α mRNA by 1.5-fold (Figure 7C), whereas it did not affect two control mRNAs: Rck, which does not contain a CDE, and Nfkbid, whose tandem CDEs lack sequence complementarity to CDE-MO-2 outside of the stems. The extent to which CDE-MO-2 increased TNF-α mRNA expression was similar to the effect of Roquin kd (1.7-fold; Figure S7H). It is important to note that CDE-MO-2 also elevated expression of TNF-α mRNA and protein in mouse primary bone marrow-derived macrophages (BMDM; Figure 7D). Because the MO approach was effective in primary cells, interfering with structured RNA motifs in *trans* may represent a future strategy to influence inflammatory responses in a therapeutic setting.

DISCUSSION

In this study, we define CDEs as a class of regulatory motifs that mediate mRNA degradation through their interaction with Roquin proteins. The active CDE is a stem-loop, as determined in vitro by in-line probing of variants that differ in their decay activity (Figures 1B and S2) and by the functional analysis of compensatory mutations (Figures 2A, 2B, and S3D). Notably, the CDE stem-loop was not observed by in-line probing of the TNF-α CDE_{150} RNA, where the stem-loop is embedded in its natural sequence context (Figure S2C). In fact, ΔG of the stem-loop in its natural context is predicted to be only −6.7 kcal/mol, suggesting that this region of the 3′ UTR does not fold into a single structure but samples different conformations. Inside cells, binding of Roquin is likely to stabilize the CDE in the stem-loop conformation.

Despite its low thermodynamic stability, the CDE bears features that are characteristic for trinucleotide hairpins. First, stable trinucleotide loops have a strong preference for Us at each position of the loop (Shu and Bevilacqua, 1999), and indeed UGU is by far the most frequently observed CDE loop (Table S4). Second, the closing base pair below the loop has an overwhelming preference for C–G in stable trinucleotide hairpins with a ΔG three times greater than that of the next best closing base pair G–C (Shu and Bevilacqua, 1999). Because the closing base pair in the CDE needs to be C–G according to our mutational analysis (Figure 2A), it matches the thermodynamically most stable configuration of trinucleotide hairpins.

Our EMSA experiments showed that Roquin binds directly and with high specificity to the CDE stem-loop (Figure 3F). Consistent with previous reports (Athanasopoulos et al., 2010; Glasmacher et al., 2010), the ROQ domain is responsible for RNA binding (Figures 3D and 3E). Overexpression of Roquin or Roquin2 accelerates CDE-mediated mRNA decay (Figures 4A and S4G–S4J), whereas the simultaneous kd of both proteins is necessary to prevent CDE mRNA degradation effectively in NIH 3T3 cells (Figures 4B and S5B). This indicates that the two proteins can induce mRNA degradation independently. In

(F) Top: binding of recombinant Roquin-N (amino acids [aa] 2–440) to the CDE_{23} RNA was examined in vitro by EMSA. Radiolabeled CDE_{23}, CDE_{23}-M23, and TNF-α-ARE RNAs were incubated with increasing concentrations of Roquin-N. Free RNA (black arrow) was separated from RNA-protein complexes (white arrow) by native PAGE. Bottom left: RNAs used for EMSA. Bottom right: the apparent dissociation constant K_d ± SE was calculated from quantification of three independent experiments.
See also Figure S4 and Table S2.

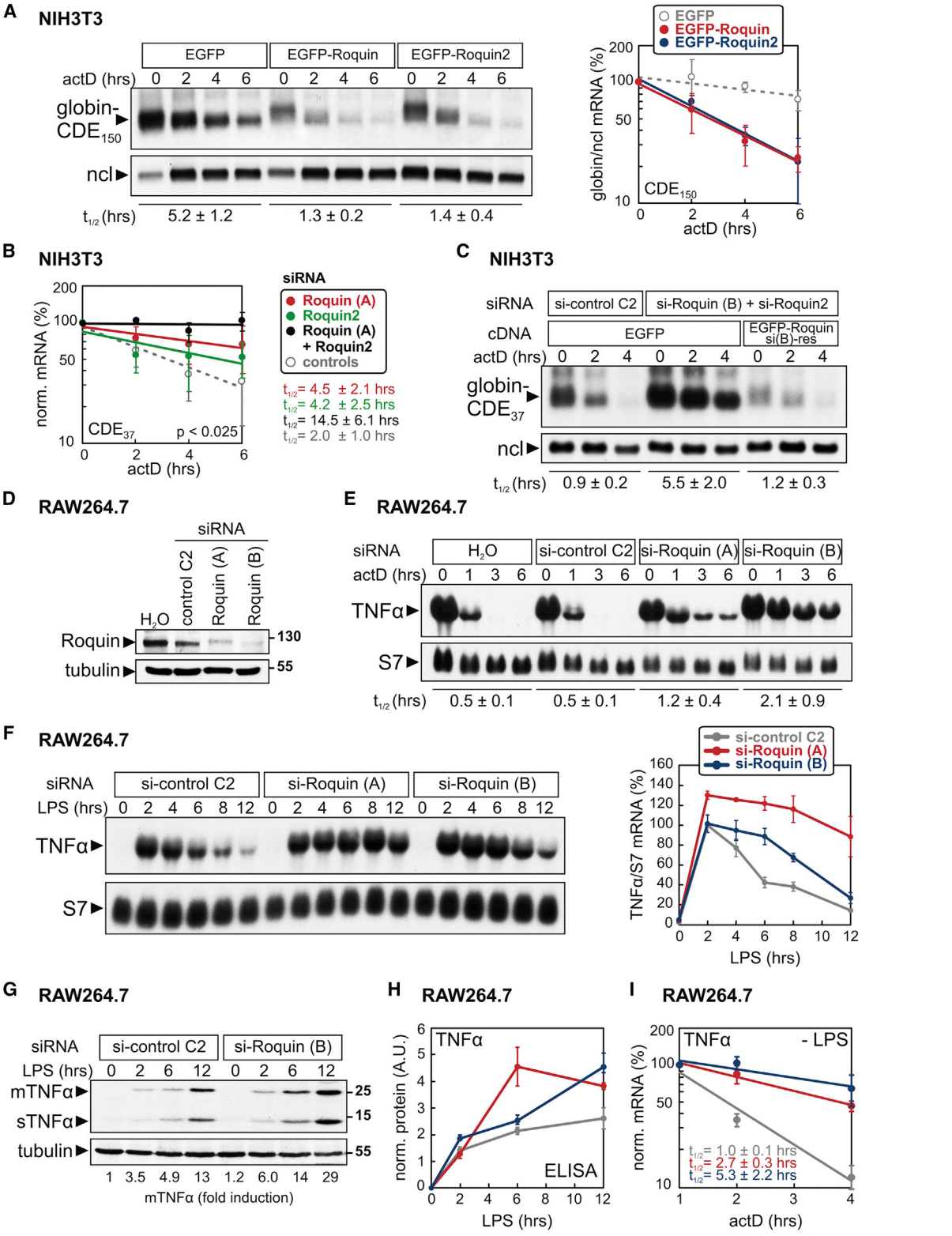

Figure 4. Roquin Is Required for CDE-Mediated mRNA Degradation

(A) Left: NIH 3T3 cells were transiently transfected with EGFP, EGFP-Roquin, or -Roquin2 together with globin-TNF-α-CDE_{150}. Reporter mRNA degradation was measured as in Figure 1E; average $t_{1/2} \pm$ SD, n ≥ 3. Right: decay curves show average (±SD) globin-TNF-α-CDE_{150} mRNA levels normalized to ncl mRNA as percentage of the initial value.

(legend continued on next page)

LPS-stimulated RAW264.7 macrophages, kd of Roquin alone is sufficient to cause stabilization and prolonged production of endogenous TNF-α mRNA, which translates into elevated synthesis of TNF-α protein (Figures 4D–4H). In macrophages, double kd of Roquin and Roquin2 did not show a greater effect (Figures S5D–S5F), suggesting that the relative importance of Roquin and Roquin2 may differ between cell types. By introducing an antisense MO that targets the TNF-α CDE and interferes with Roquin binding in *trans*, we observed elevated expression of TNF-α in RAW264.7 macrophages and primary BMDM (Figures 7A–7D). Taken together, these results demonstrate that Roquin acts through the CDE as a suppressor of TNF-α expression in macrophages. This might be different in T cells, where overexpression of Roquin was found to cause elevated levels of numerous proinflammatory cytokines, including TNF-α (Ji et al., 2012).

By affinity purification of Roquin and Roquin2, we found that both proteins are associated with the entire Ccr4-Caf1-Not complex (Table S3). Co-IP experiments revealed that the interaction of Roquin and Roquin2 with Not1 and the deadenylase Caf1a is RNA independent and occurs through the C-terminal region of Roquin (Figure 5). Importantly, a catalytically inactive Caf1a mutant potently inhibited CDE mRNA deadenylation and degradation. We propose that Roquin and Roquin2 serve as adaptor proteins that specifically recognize CDE-like RNA stem-loops via the ROQ domain and destabilize their target mRNAs by recruitment of the Ccr4-Caf1-Not deadenylase complex via the C-terminal effector domain (Figure 7E).

Using our experimentally derived consensus CDE sequence and structure (Figure 6A), we identified 56 highly conserved CDEs in the 3′ UTRs of 55 vertebrate genes (Table S4). By an in silico approach, Parker et al. (2011) predicted novel families of structured motifs within mRNAs, including several stem-loops that correspond to CDEs, supporting the notion that the CDE is a widespread regulatory element. Through the genome-wide identification of Roquin target mRNAs (Table S6), we found that mRNAs with conserved CDEs are strongly enriched by Roquin IP (Figure 6C). In fact, the highest enrichment was observed for the only mouse mRNA (Nfkbid) that contains a tandem CDE motif in its 3′ UTR. Similarly, the only two mouse mRNAs containing two CDEs in their open reading frame (ORF) (D5Ertd579e and Ipo11) showed strongest enrichment by Roquin IP among all mRNAs with ORF CDEs. These results demonstrate that the CDE is the principal Roquin binding element.

Roquin was previously found to suppress the expression of ICOS, a costimulatory receptor for follicular T helper cells, by accelerating ICOS mRNA degradation (Glasmacher et al., 2010; Yu et al., 2007). *Sanroque* mice contain a single amino acid substitution (M199R) in Roquin and display a lupus-like autoimmune syndrome, which was proposed to result from the elevated expression of ICOS (Vinuesa et al., 2005). We did not observe a difference between wild-type Roquin and the M199R mutant with regard to CDE binding or acceleration of CDE mRNA decay (data not shown). Also, a more recent study reported that the knockout of Roquin in the hematopoietic system did not cause autoimmunity but led to a more inflammatory phenotype dominated by the expansion of eosinophilic granulocytes, macrophages, and CD8 effector-like T cells (Bertossi et al., 2011). Our genome-wide identification of Roquin targets (Table S6) revealed several immunity- and inflammation-related mRNAs, including TNF-α and three regulators of the NF-κB pathway: Nfkbid, a member of the IκB family of NF-κB inhibitors, Nfkbiz, a nuclear member of the same family, and Ier3, a protein that stabilizes IκBα (Arlt and Schäfer, 2011; Renner and Schmitz, 2009). Given that an estimated additional 50 mRNAs are likely to contain functional CDEs (Table S4), and that 95 mRNAs were significantly enriched by Roquin IP (Table S6), we postulate that the complex phenotypes of the hematopoietic Roquin knockout and *sanroque* mice may, in fact, arise from the simultaneous deregulation of multiple mRNAs in the immune system. The complete knockout of Roquin causes perinatal lethality and malformations of the tail and spinal column (Bertossi et al., 2011). This phenotype may be linked to our observation that 13 mRNAs encoding regulators of development, including Wnt3a and Bmpr1a, contain highly conserved CDEs (Tables S4 and S5). Six of these mRNAs, including Bmpr1a, were also enriched by Roquin IP (Table S6). It is interesting that 10 of the CDEs we identified are conserved between fish and mammals, suggesting that Roquin-mediated mRNA regulation is maintained among vertebrates. Because Roquin homologs are found in all branches of metazoan evolution, Roquin-CDE interactions may have an ancient role in multicellular organisms.

(B) The kd of Roquin and Roquin2, either alone or in combination, was combined with transient expression of globin-TNF-α-CDE_{37}-V3 in NIH 3T3 cells. Reporter mRNA decay rates were quantified from northern blots; average $t_{1/2} \pm$ SD, $n \geq 3$. The p value was calculated by one-sided t test for the comparison of $t_{1/2}$ between double Roquin/Roquin2 kd and combined controls. A corresponding northern blot is depicted in Figure S5B.
(C) EGFP or siRNA-resistant EGFP-Roquin-si(B)-res was transfected into NIH 3T3 cells 1 day after transfection of control siRNA C2 or siRNAs against Roquin [si-Roquin (B)] and Roquin2. Degradation of globin-TNF-α-CDE_{37}-V3 reporter mRNA was measured on day 2 as in Figure 1E; average $t_{1/2} \pm$ SD, n = 3.
(D) RAW264.7 cells were transfected twice over a period of 2 days with water (H_2O), control siRNA (C2), or two different siRNAs against Roquin (A) and (B). Roquin protein levels were assessed by western blot analysis.
(E) RAW264.7 cells were transfected with siRNAs as in (D) and stimulated with LPS (100 ng/ml) for 2 hr prior to addition of actD. Endogenous TNF-α mRNA decay was measured by northern blot analysis using ribosomal protein S7 mRNA as loading control; average $t_{1/2} \pm$ SD, n = 3.
(F) Left: TNF-α mRNA expression in response to LPS was analyzed by northern blot in RAW264.7 cells subjected to Roquin or control kd. Right: quantification shows average TNF-α mRNA levels normalized to S7 mRNA (±SD, n = 3).
(G) Synthesis of membrane-bound (m)TNF-α and soluble (s)TNF-α in response to LPS was analyzed by western blot in RAW264.7 cells subjected to Roquin or control kd. Quantification of mTNF-α normalized to tubulin is shown below the blot.
(H) TNF-α secretion was measured by ELISA in the supernatants of RAW264.7 cells treated as in (F). The graph shows normalized TNF-α levels (average ± SE, n = 3).
(I) Degradation of TNF-α mRNA was measured in resting RAW264.7 macrophages by RT-qPCR after normalization to NupL1 mRNA. Shown are average values ± SD, n = 3.
See also Figures S4 and S5.

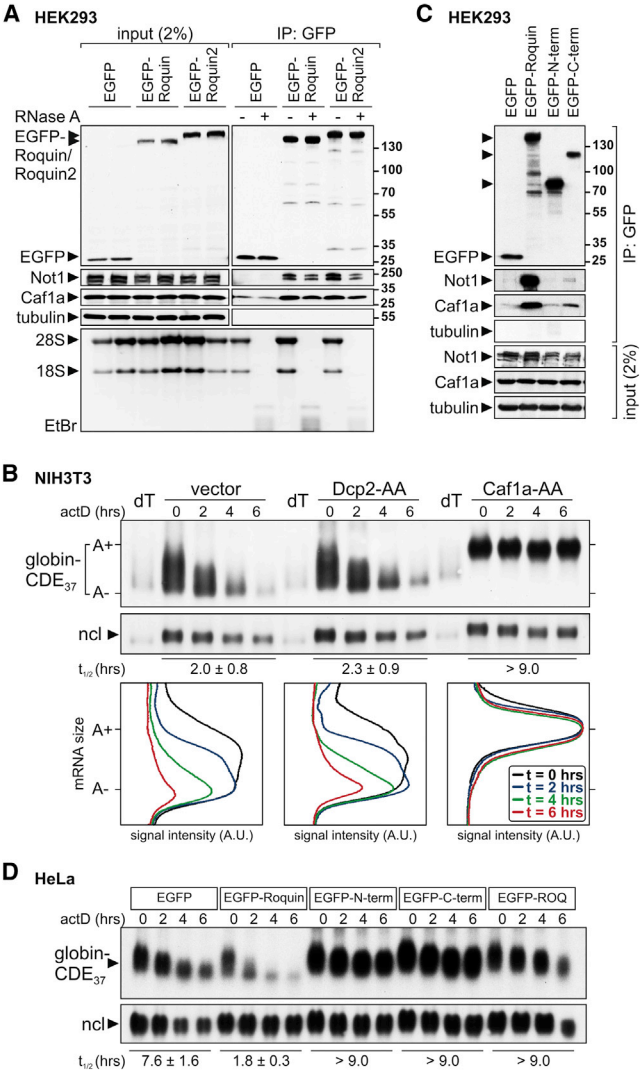

Figure 5. The CDE Induces Caf1-Dependent mRNA Deadenylation

(A) HEK293 cells were transiently transfected with EGFP, EGFP-Roquin, or -Roquin2. After EGFP IP from cytoplasmic lysates, in the presence or absence of RNase A, endogenous Not1 and Caf1a were detected by western blot analysis. Staining of ribosomal RNA by ethidium bromide (EtBr) documents efficiency of RNase treatment.

(B) Top: NIH 3T3 cells were transiently transfected with globin-TNF-α-CDE_{37}-V3 together with vector control, dominant-negative Dcp2-AA or dominant-negative Caf1a-AA. Reporter mRNA degradation was analyzed as in Figure 1E, except that RNA was resolved on a higher resolution 1.6% agarose gel. dT, treatment of RNA with oligo-dT and RNase H to remove poly(A) tails; average $t_{1/2} \pm$ SD, n = 3. Bottom: deadenylation was visualized by quantifying the signal intensity (A.U., arbitrary units) of the reporter mRNA along the length of the signal, plotted against mRNA size; A+, polyadenylated; A−, deadenylated mRNA.

(C) HEK293 cells were transiently transfected with EGFP, EGFP-tagged Roquin, N-term, or C-term. After EGFP IP from cytoplasmic lysates, endogenous Not1 and Caf1a were detected by western blot analysis.

(D) HeLa cells were transiently transfected with globin-TNF-α-CDE_{37}-V3 together with EGFP, EGFP-tagged Roquin, C-term, N-term or ROQ. Reporter mRNA degradation was analyzed as in Figure 1E; average $t_{1/2} \pm$ SD, n = 3. See also Figure S6 and Table S3.

As exemplified by TNF-α, the presence of multiple regulatory elements in the same mRNA may allow for the integration of regulatory cues from various signaling pathways. Similar to promoter regions that offer binding sites for different transcription factors, the UTRs of mRNAs are increasingly recognized as versatile regulatory platforms. Our identification of CDEs as a conserved class of RNA stem-loop motifs bound by Roquin proteins adds an important component to the complex network that governs posttranscriptional control of gene expression.

EXPERIMENTAL PROCEDURES

Detailed descriptions of methods, plasmids, and primers can be found in the Extended Experimental Procedures and Table S7.

mRNA Decay Assay

For mRNA decay experiments, 5 μg/ml actinomycin D (AppliChem) was added to the medium for the indicated time intervals before harvesting cells and extracting total RNA using the Genematrix universal RNA purification kit (Eurx, Roboklon). mRNA levels were determined either by northern blot or by RT-qPCR analysis.

In-Line Probing

For in-line probing, CDE_{37}-V2, CDE_{37}-V3, and CDE_{150} RNAs were transcribed in vitro using T7 RNA polymerase, dephosphorylated, and 5′ radiolabeled with [γ-^{32}P]ATP. The RNA was then incubated for 45 hr at pH 8.3 at room temperature, and resolved by urea-PAGE.

RNA Affinity Purification

Cytoplasmic lysates of NIH 3T3 B2A2 cells were prepared using the RNA IP lysis buffer described in the Extended Experimental Procedures. 4xS1m and CDE_{37}-4xS1m RNAs were transcribed in vitro and precoupled to streptavidin sepharose (GE Healthcare). After incubation of the precleared lysate with the RNA matrix, the beads were washed and proteins were eluted with RNase A (Genomed). The eluate was concentrated by vacuum centrifugation for SDS-PAGE and subsequent mass spectrometry analysis.

EGFP-Roquin Affinity Purification

HEK293 cell lines stably expressing tetracycline-inducible EGFP-Roquin or EGFP-Roquin2 were lysed mechanically, and the cleared cytoplasmic lysates were subjected to ultracentrifugation at 100,000 × *g*. Pellets were resuspended and incubated with sepharose-coupled GFP binder. Finally, proteins were SDS-eluted from the matrix and analyzed by mass spectrometry.

RNA IP, Library Preparation, Deep Sequencing, and Data Analysis

Endogenous Roquin was immunoprecipitated from lysates of RAW246.7 macrophages stimulated for 2 hr with LPS (100 ng/ml). Beads alone served as control. RNA was extracted from IP and input samples using TriFast (PeqLab). Library preparation was carried out with Illumina protocols using 50–100 ng RNA. Sequencing was performed on an Illumina HiSeq2000 instrument, which yielded a raw read length of 58 bases. Reads were aligned to the *Mus musculus* genome, and differential expression was tested using Bioconductor software. A detailed description and references can be found in the Extended Experimental Procedures.

ACCESSION NUMBERS

RNA sequencing data from Roquin IP experiments were deposited in the Gene Expression Omnibus under accession number GSE44775.

SUPPLEMENTAL INFORMATION

Supplemental Information includes Extended Experimental Procedures, seven figures, and seven tables and can be found with this article online at http://dx.doi.org/10.1016/j.cell.2013.04.016.

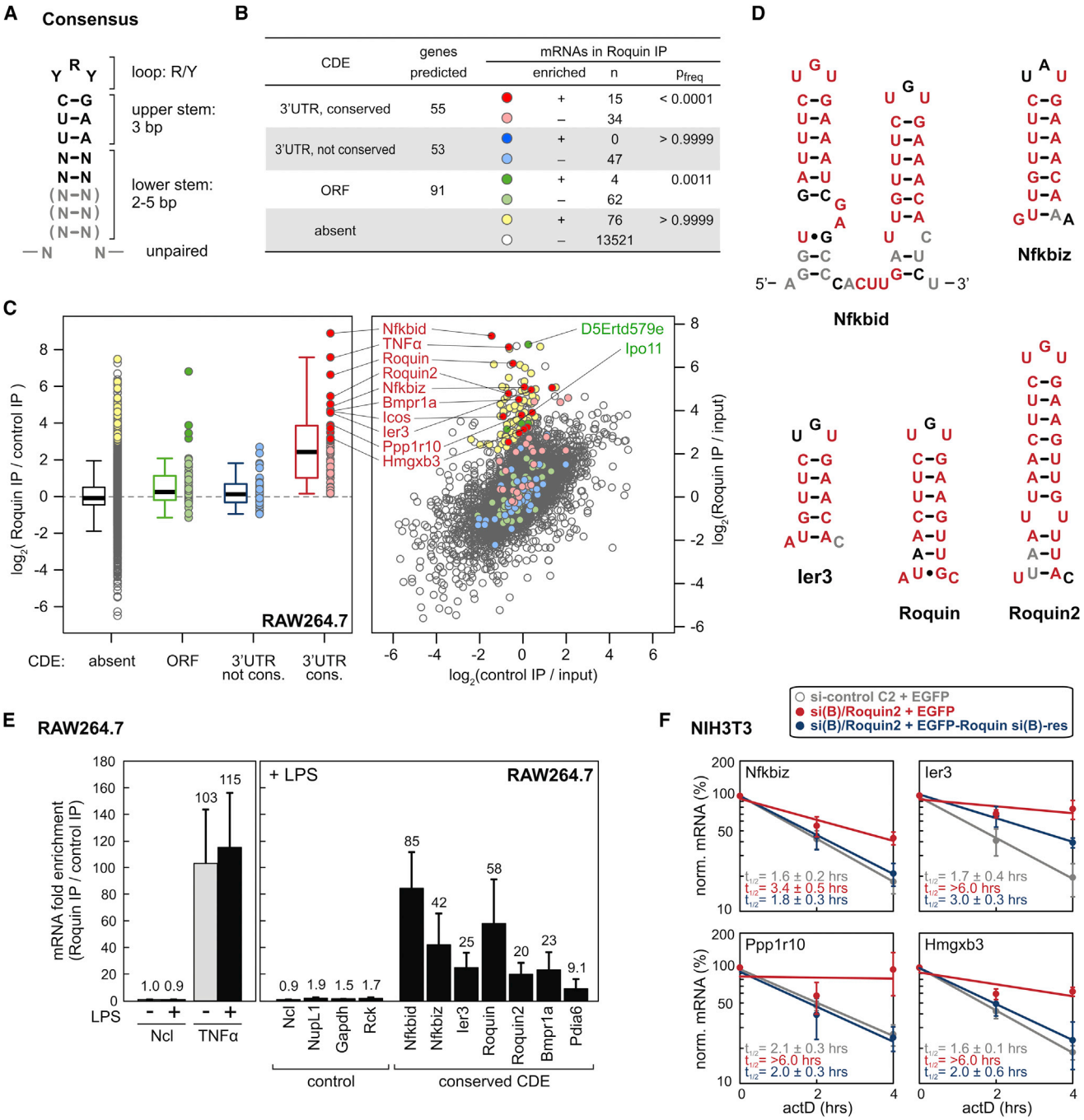

Figure 6. Genome-wide Identification of CDEs and Roquin Target mRNAs

(A) Consensus CDE stem-loop motif used for bioinformatics prediction of CDE-containing mRNAs.

(B) Numbers of genes predicted to contain a CDE and corresponding mRNAs significantly enriched by Roquin IP from LPS-stimulated RAW264.7 macrophages. Significant enrichment is defined by a p value $\leq$ 0.005 (Roquin IP versus control IP) and fold enrichment (Roquin IP/control IP) > 8.0. p_{freq} represents the hypergeometric probability of randomly finding at least the observed number of mRNAs enriched by Roquin IP in each of the four groups of mRNAs, given the overall frequency of 95 significantly enriched mRNAs in a total of 13,759 mRNAs.

(C) mRNAs associated with Roquin in LPS-stimulated RAW264.7 macrophages were recovered by RNA IP and identified by RNA sequencing, n = 3. Left: average enrichment (Roquin IP/control IP) is plotted for all Reference Sequence database (RefSeq)-annotated protein-coding transcripts; these transcripts are grouped according to the bioinformatics prediction of CDEs. Right: enrichment over input is depicted for the same transcripts. The color code refers to (B).

(D) Secondary structures predicted for conserved CDEs. Based on the University of California, Santa Cruz (UCSC), genome alignment, nts are color coded according to conservation as in Figure 1D.

(legend continued on next page)

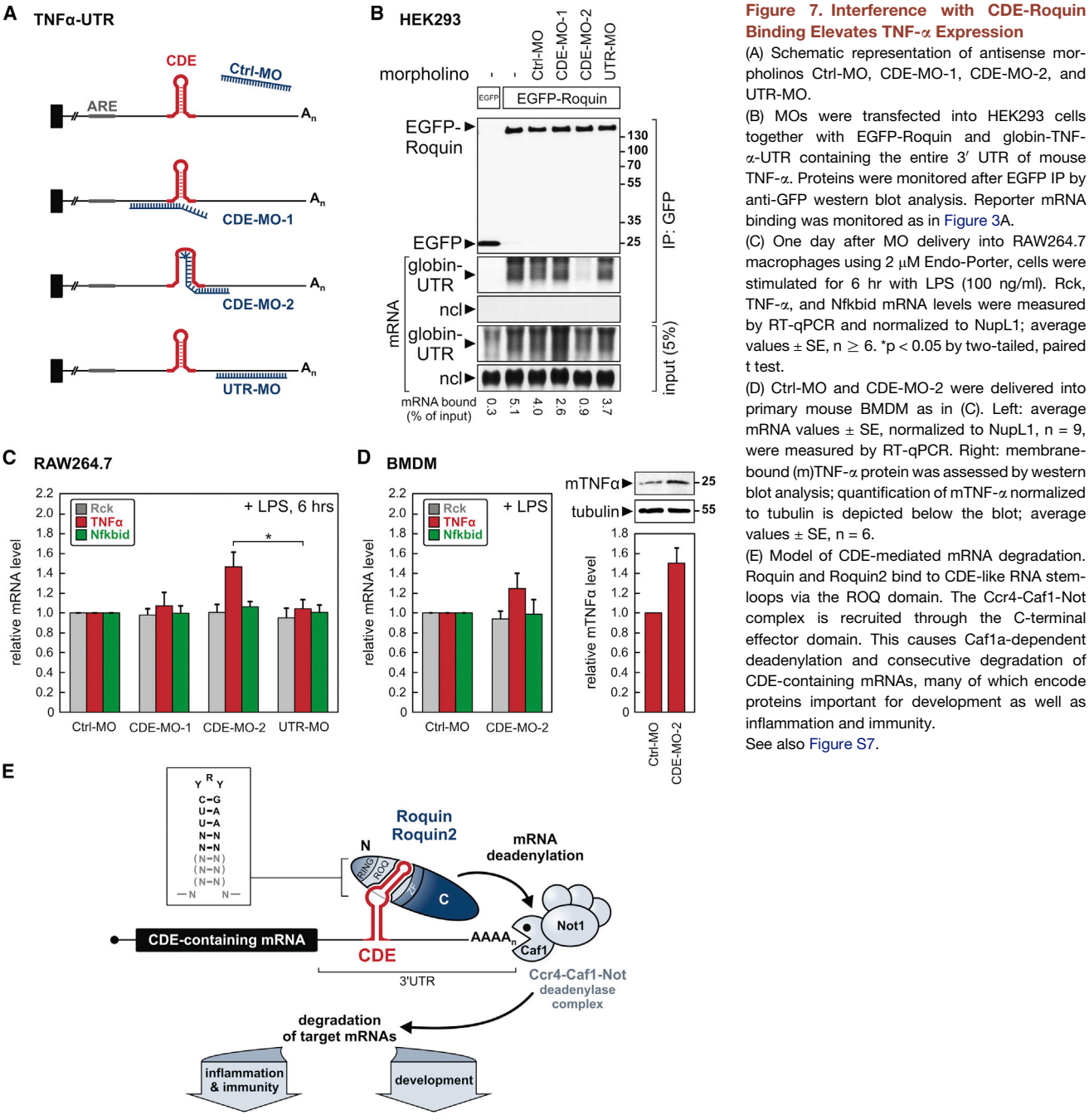

Figure 7. Interference with CDE-Roquin Binding Elevates TNF-α Expression

(A) Schematic representation of antisense morpholinos Ctrl-MO, CDE-MO-1, CDE-MO-2, and UTR-MO.

(B) MOs were transfected into HEK293 cells together with EGFP-Roquin and globin-TNF-α-UTR containing the entire 3′ UTR of mouse TNF-α. Proteins were monitored after EGFP IP by anti-GFP western blot analysis. Reporter mRNA binding was monitored as in Figure 3A.

(C) One day after MO delivery into RAW264.7 macrophages using 2 μM Endo-Porter, cells were stimulated for 6 hr with LPS (100 ng/ml). Rck, TNF-α, and Nfkbid mRNA levels were measured by RT-qPCR and normalized to NupL1; average values ± SE, n ≥ 6. *p < 0.05 by two-tailed, paired t test.

(D) Ctrl-MO and CDE-MO-2 were delivered into primary mouse BMDM as in (C). Left: average mRNA values ± SE, normalized to NupL1, n = 9, were measured by RT-qPCR. Right: membrane-bound (m)TNF-α protein was assessed by western blot analysis; quantification of mTNF-α normalized to tubulin is depicted below the blot; average values ± SE, n = 6.

(E) Model of CDE-mediated mRNA degradation. Roquin and Roquin2 bind to CDE-like RNA stem-loops via the ROQ domain. The Ccr4-Caf1-Not complex is recruited through the C-terminal effector domain. This causes Caf1a-dependent deadenylation and consecutive degradation of CDE-containing mRNAs, many of which encode proteins important for development as well as inflammation and immunity.

See also Figure S7.

ACKNOWLEDGMENTS

We would like to thank Bernd Rattenbacher and Christoph Moroni (University of Basel, Basel, Switzerland) for sharing unpublished information. We are grateful to Vigo Heissmeyer (Helmholtz Center Munich, Munich, Germany) for providing the Dicer mouse embryonic fibroblasts (MEFs) and the plasmids encoding EGFP-Roquin and His-Roquin-N; Witold Filipowicz (Friedrich Miescher Institute for Biomedical Research, Basel, Switzerland) for the Dicer

(E) Binding of mRNAs to Roquin by RNA IP analysis. Left: TNF-α mRNA was quantified by RT-qPCR after IP of endogenous Roquin from RAW264.7 macrophages with or without stimulation for 2 hr with LPS (100 ng/ml). The signal was divided by the amount of TNF-α mRNA in the control IP and expressed as fold enrichment (average ± SE, n ≥ 7). Right: average enrichment ± SE (n ≥ 3) of four control mRNAs and seven mRNAs containing conserved CDEs.

(F) Degradation of the CDE-containing Nfkbiz, Ier3, Ppp1r10, and Hmgxb3 mRNAs was measured by quantitative RT-qPCR in NIH 3T3 cells after control kd (siRNA C2), kd of Roquin/Roquin2, and rescue by siRNA-resistant Roquin. All mRNA levels were normalized to NupL1 mRNA; average $t_{1/2}$ ± SE, n = 3.

See also Figure S7 as well as Tables S4, S5, and S6.

antibody; Ann-Bin Shyu (University of Texas Medical School at Houston, Houston, TX, USA) for the Caf1a antibody and the NIH 3T3 B2A2 cell line; Takbum Ohn, Nancy Kedersha, and Paul Anderson (Harvard Medical School, Boston, MA, USA) for Flag-Roquin plasmids; Adelheid Cerwenka (German Cancer Research Center, Heidelberg, Germany) for providing mouse bone marrow; Ivana Cado for generating stable cell lines; and Alexandra Kurz (German Cancer Research Center, Heidelberg) for help with ELISA. We would like to thank David Ibberson and Sasithorn Chotewutmontri of the Heidelberg University Deep Sequencing Core Facility, the Genomics Core Facility at the European Molecular Biology Laboratory, and Thomas Ruppert from the ZMBH (Zentrum für Molekulare Biologie der Universität Heidelberg) Mass Spectrometry Core Facility for extensive support. We also thank Ingrid Grummt and Aurelio Teleman (German Cancer Research Center, Heidelberg) for critical reading of the manuscript. This work was supported by Young Investigator Grant HZ-NG-210 from the Helmholtz Gemeinschaft to G.S.; SFB 1036/TP07 as well as research grants STO 859/2-1 and STO 859/3-1 from the Deutsche Forschungsgemeinschaft to G.S.; a PhD stipend from the Helmholtz International Graduate School for Cancer Research to K.L.; and a CASI (Career Awards at the Scientific Interface) award from the Burroughs Wellcome Fund to M.C.H. K.L. designed and performed experiments, analyzed the data, prepared figures, and cowrote the manuscript; J.S. carried out bioinformatics analysis and performed experiments; S.R. and F.P. performed experiments; M.C.H. performed in-line probing; and G.S. supervised the study, designed experiments, analyzed the data, and cowrote the manuscript.

Received: January 14, 2012
Revised: December 7, 2012
Accepted: April 5, 2013
Published: May 9, 2013

REFERENCES

Androulidaki, A., Iliopoulos, D., Arranz, A., Doxaki, C., Schworer, S., Zacharioudaki, V., Margioris, A.N., Tsichlis, P.N., and Tsatsanis, C. (2009). The kinase Akt1 controls macrophage response to lipopolysaccharide by regulating microRNAs. Immunity *31*, 220–231.

Arlt, A., and Schäfer, H. (2011). Role of the immediate early response 3 (IER3) gene in cellular stress response, inflammation and tumorigenesis. Eur. J. Cell Biol. *90*, 545–552.

Athanasopoulos, V., Barker, A., Yu, D., Tan, A.H., Srivastava, M., Contreras, N., Wang, J., Lam, K.P., Brown, S.H., Goodnow, C.C., et al. (2010). The ROQUIN family of proteins localizes to stress granules via the ROQ domain and binds target mRNAs. FEBS J. *277*, 2109–2127.

Bertossi, A., Aichinger, M., Sansonetti, P., Lech, M., Neff, F., Pal, M., Wunderlich, F.T., Anders, H.J., Klein, L., and Schmidt-Supprian, M. (2011). Loss of Roquin induces early death and immune deregulation but not autoimmunity. J. Exp. Med. *208*, 1749–1756.

Bradley, J.R. (2008). TNF-mediated inflammatory disease. J. Pathol. *214*, 149–160.

Carballo, E., Lai, W.S., and Blackshear, P.J. (1998). Feedback inhibition of macrophage tumor necrosis factor-alpha production by tristetraprolin. Science *281*, 1001–1005.

Chen, C.Y., Gherzi, R., Ong, S.E., Chan, E.L., Raijmakers, R., Pruijn, G.J., Stoecklin, G., Moroni, C., Mann, M., and Karin, M. (2001). AU binding proteins recruit the exosome to degrade ARE-containing mRNAs. Cell *107*, 451–464.

Collart, M.A., and Panasenko, O.O. (2012). The Ccr4—not complex. Gene *492*, 42–53.

Fenger-Grøn, M., Fillman, C., Norrild, B., and Lykke-Andersen, J. (2005). Multiple processing body factors and the ARE binding protein TTP activate mRNA decapping. Mol. Cell *20*, 905–915.

Garneau, N.L., Wilusz, J., and Wilusz, C.J. (2007). The highways and byways of mRNA decay. Nat. Rev. Mol. Cell Biol. *8*, 113–126.

Glasmacher, E., Hoefig, K.P., Vogel, K.U., Rath, N., Du, L., Wolf, C., Kremmer, E., Wang, X., and Heissmeyer, V. (2010). Roquin binds inducible costimulator mRNA and effectors of mRNA decay to induce microRNA-independent post-transcriptional repression. Nat. Immunol. *11*, 725–733.

Goodarzi, H., Najafabadi, H.S., Oikonomou, P., Greco, T.M., Fish, L., Salavati, R., Cristea, I.M., and Tavazoie, S. (2012). Systematic discovery of structural elements governing stability of mammalian messenger RNAs. Nature *485*, 264–268.

Hao, S., and Baltimore, D. (2009). The stability of mRNA influences the temporal order of the induction of genes encoding inflammatory molecules. Nat. Immunol. *10*, 281–288.

Huntzinger, E., and Izaurralde, E. (2011). Gene silencing by microRNAs: contributions of translational repression and mRNA decay. Nat. Rev. Genet. *12*, 99–110.

Ji, Y.R., Kim, H.J., Yu, D.H., Bae, K.B., Park, S.J., Yi, J.K., Kim, N., Park, S.J., Oh, K.B., Hwang, S.S., et al. (2012). Enforced expression of roquin protein in T cells exacerbates the incidence and severity of experimental arthritis. J. Biol. Chem. *287*, 42269–42277.

Marzluff, W.F., Wagner, E.J., and Duronio, R.J. (2008). Metabolism and regulation of canonical histone mRNAs: life without a poly(A) tail. Nat. Rev. Genet. *9*, 843–854.

Matsushita, K., Takeuchi, O., Standley, D.M., Kumagai, Y., Kawagoe, T., Miyake, T., Satoh, T., Kato, H., Tsujimura, T., Nakamura, H., and Akira, S. (2009). Zc3h12a is an RNase essential for controlling immune responses by regulating mRNA decay. Nature *458*, 1185–1190.

Parker, B.J., Moltke, I., Roth, A., Washietl, S., Wen, J., Kellis, M., Breaker, R., and Pedersen, J.S. (2011). New families of human regulatory RNA structures identified by comparative analysis of vertebrate genomes. Genome Res. *21*, 1929–1943.

Rabani, M., Levin, J.Z., Fan, L., Adiconis, X., Raychowdhury, R., Garber, M., Gnirke, A., Nusbaum, C., Hacohen, N., Friedman, N., et al. (2011). Metabolic labeling of RNA uncovers principles of RNA production and degradation dynamics in mammalian cells. Nat. Biotechnol. *29*, 436–442.

Renner, F., and Schmitz, M.L. (2009). Autoregulatory feedback loops terminating the NF-kappaB response. Trends Biochem. Sci. *34*, 128–135.

Sandler, H., Kreth, J., Timmers, H.T., and Stoecklin, G. (2011). Not1 mediates recruitment of the deadenylase Caf1 to mRNAs targeted for degradation by tristetraprolin. Nucleic Acids Res. *39*, 4373–4386.

Schwanhäusser, B., Busse, D., Li, N., Dittmar, G., Schuchhardt, J., Wolf, J., Chen, W., and Selbach, M. (2011). Global quantification of mammalian gene expression control. Nature *473*, 337–342.

Shu, Z., and Bevilacqua, P.C. (1999). Isolation and characterization of thermodynamically stable and unstable RNA hairpins from a triloop combinatorial library. Biochemistry *38*, 15369–15379.

Srisawat, C., and Engelke, D.R. (2001). Streptavidin aptamers: affinity tags for the study of RNAs and ribonucleoproteins. RNA *7*, 632–641.

Stoecklin, G., Lu, M., Rattenbacher, B., and Moroni, C. (2003). A constitutive decay element promotes tumor necrosis factor alpha mRNA degradation via an AU-rich element-independent pathway. Mol. Cell. Biol. *23*, 3506–3515.

Tracey, K.J., and Cerami, A. (1994). Tumor necrosis factor: a pleiotropic cytokine and therapeutic target. Annu. Rev. Med. *45*, 491–503.

Vinuesa, C.G., Cook, M.C., Angelucci, C., Athanasopoulos, V., Rui, L., Hill, K.M., Yu, D., Domaschenz, H., Whittle, B., Lambe, T., et al. (2005). A RING-type ubiquitin ligase family member required to repress follicular helper T cells and autoimmunity. Nature *435*, 452–458.

Yu, D., Tan, A.H., Hu, X., Athanasopoulos, V., Simpson, N., Silva, D.G., Hutloff, A., Giles, K.M., Leedman, P.J., Lam, K.P., et al. (2007). Roquin represses autoimmunity by limiting inducible T-cell co-stimulator messenger RNA. Nature *450*, 299–303.

EXTENDED EXPERIMENTAL PROCEDURES

Cell Culture and Transfection

MEFs as well as NIH 3T3, HeLa, HEK293T and RAW264.7 cells were cultured in Dulbecco's Modified Eagle's Medium (DMEM, GIBCO) supplemented with 10% fetal calf serum (PAA Laboratories), 2 mM L-glutamine, 100 U/ml penicillin and 0.1 mg/ml streptomycin (all PAN Biotech) at 37°C in 5% CO_2. BMDM were isolated from the femur and tibia of wild-type (WT) C57BL/6 mice as described previously (Stoecklin et al., 2008). BMDM were cultured for 10–12 days in DMEM supplemented with 10% fetal calf serum (Sigma), 20 mM HEPES (PAA), 2 mM L-glutamine (PAN Biotech) essential and nonessential amino acids (Invitrogen), 55 μM 2-mercaptoethanol (Sigma), 100 units/ml penicillin (PAN Biotech), 100 μg/ml streptomycin (PAN Biotech) and 20% conditioned medium from L929 cells as a source of macrophage colony-stimulating-factor. Dicer MEFs (Glasmacher et al., 2010) were kindly provided by Vigo Heissmeyer (Helmholtz Center Munich, Germany) with permission from Gregory J. Hannon (Cold Spring Harbor Laboratory, New York, USA), and NIH 3T3 B2A2 cells (Xu et al., 1998) were a generous gift from Ann-Bin Shyu (University of Texas-Houston Medical School). NIH 3T3, HeLa, HEK293T cells were seeded in 10-cm dishes and transfected the following day with 10–12 μg of plasmid using polyethyleneimine (PEI, Polysciences Europe, 1 mg/ml, pH 7.0 at 25°C) at a ratio of 1:2 (DNA:PEI) in serum-free and antibiotic-free DMEM. The medium was changed to regular DMEM 4-6 hr after transfection. Stable MEF cell lines were generated by nucleofection (Amaxa) and subsequent selection with G418 (400 μg/ml, AppliChem). Where indicated, RAW264.7 cells were treated with LPS (100 ng/ml, Sigma, L2630, *E. coli* serotype O111:B4).

Plasmid Construction

The following plasmids have been described previously: puroMXβglobin (p2220, also referred to as puroMXβ) containing the rabbit β-globin reporter gene driven by the Moloney murine leukemia virus (MMLV) promoter (Stoecklin et al., 2001); puroMXβ-TNF-α-KΔAU (p2230) (Stoecklin et al., 2003); pEGFP-N1 (Clontech/ BD Biosciences); pLNCX2-EGFP-Roquin (p2838) encoding EGFP-tagged full-length mouse Roquin and pETM11-Roquin-N (p2940) for expression of His-Roquin-N (aa 2-440) (Glasmacher et al., 2010); TOPuro-Caf1a-mycSG (p2485) and TOPuro-Caf1a-AA-mycSG (p2737) encoding human WT Caf1a and the dominant negative D40A/E42A mutant, respectively; pcDNA3-Flag (p2002) and pcDNA3-Flag-Dcp2-AA (p2798) harboring the E147A/E148A Dcp2 mutant (Ozgur et al., 2010); as well as pCMV-Flag-Not1 (p2556) encoding Not1 (Winkler et al., 2006).

For pcDNA3-GFβ (p2732), which encodes a GFP/β-globin fusion protein, EGFP was amplified with primers G1612/G1613 (Table S7, all oligonucleotides were purchased from Invitrogen or Eurofins MWG Operon) and cloned as a *Hind*III–*Kpn*I fragment into the *Hind*III/*Kpn*I sites of pcDNA3-7B (p2308) (Ozgur et al., 2010). pcDNA3-GFβ-TNF-α-CDE (p2730), was generated by insertion of annealed oligonucleotides spanning a 14 nt linker (*Nhe*I, *Age*I sites) and the 40 nt CDE of mouse TNF-α (see Table S1 for all CDE inserts). The oligonucleotides were designed with *Bam*HI- and *Bgl*II-compatible ends, 5′-phosphorylated using T4 polynucleotide kinase (Promega) and annealed prior to ligation into the *Bgl*II site of pcDNA3-GFβ (p2732), whereby a 5′-*Bam*HI/*Bgl*II fusion site (AGATCC) and a 3′-*Bgl*II site were created. For puroMXβ-TNF-α-CDE (p2812), the CDE was excised as an *Eco*RI–*Bgl*II fragment from pcDNA3-GFβ-TNF-α-CDE (p2730) and ligated into the *Eco*RI/*Bgl*II sites of puroMXβ (p2220).

By the same *Bam*HI-*Bgl*II strategy, annealed oligonucleotides were inserted into the *Bgl*II-site of puroMXβ (p2220) to generate the following plasmids: puroMXβ-TNF-α-CDE_{37}-V2 (p2814), -V3 (p2823), -V3-M1 (p2825), -V3-M2 (p2826), -V3-M3 (p2827), -V3-M4 (p2828), -V3-M5 (p2829), -V3-M6 (p2830), -V3-M7 (p2831), -V3-M8 (p2832), -V3-M9 (p2833), -V3-M10 (p2834), -V3-M11 (p2835), -V3-M12 (p2859), -V3-M13 (p2860), -V3-M14 (p2861), -V3-M15 (p2862), -V3-M16 (p2863), -V3-M17 (p2864), -V3-M18 (p2944), -V3-M19 (p2945), -V3-M20 (p2959), -V3-M21 (p2946), -V3-M22 (p2947), -V3-M23 (p2960), -V3-M24 (p2961), -V3-M25 (p2948), -V3-M26 (p2967), -V3-M27 (p2968), puroMXβ-TNF-α-CDE_{17}-ds (p2966) and puroMXβ-human-TNF-α-CDE_{37}-V3 (p2836). All CDE sequences and corresponding mRNA half-lives are summarized in Table S1.

In order to generate puroMXβ-TNF-α-CDE_{17}-ss (p2965) and puroMXβ-ICOS-CDE_{17}-ss (p2991), puroMXβ was engineered to contain an *Xba*I, *Age*I and *Nhe*I site between the β-globin stop codon and the *Bgl*II site, and CDE_{17}-containing oligos with *Xba*I- and *Age*I-compatible ends were ligated into the *Xba*I/*Age*I sites. For puroMXβ-TNF-α-CDE_{150} (p2969), a 150 nt fragment of the mouse TNF-α 3′UTR containing the CDE in its center was amplified using *Bam*HI- and *Bgl*II-linkered primers (G2495/G2496) and cloned into the *Bgl*II site of puroMXβ (p2220). Mutations in puroMXβ-TNF-α-CDE_{150}-M16 (p2970) and puroMXβ-TNF-α-CDE_{150}-M20 (p2972) were generated by the following PCR strategy: up- and downstream portions of the CDE_{150} were amplified using mutation-bearing primers (G2495/G2498 and G2497/G2496 for M16, G2495/G2502 and G2501/G2496 for M20), annealed, and the full CDE_{150} fragment was reamplified with G2495/G2496 prior to insertion into the *Bgl*II site of puroMXβ (p2220). Plasmids containing the affinity tag 4xS1m will be described in detail elsewhere. The TNF-α mouse 3′UTR was ligated into puroMXβ (p2220) as a *Sal*I/*Bgl*II fragment from pBABEpuro-GFP-TNF-α-UTR (G. Stoecklin, unpublished) to generate puroMXβ-TNF-α-3′UTR (p2914).

A point mutation in the Roquin2 cDNA obtained from Imagenes was replaced with a WT fragment amplified by PCR from mouse cDNA with primers G2421/G2427. The full-length Roquin2 cDNA was then cloned as a *Sal*I–*Cla*I fragment into pLNCX2 (Clontech) to generate pLNCX2-Roquin2 (p2984). For pLNCX2-EGFP-Roquin2 (p2985), EGFP was excised using *Sal*I from pLNCX2-EGFP-Roquin (p2838) and inserted into the *Sal*I site of pLNCX2-Roquin2 (p2984). The Roquin and Roquin2 zinc finger mutants were generated replacing the first cysteine in the CCCH-type zinc finger domains of both proteins with an arginine, resulting in a RCCH motif (Roquin-C419R and Roquin2-C416R). Mutagenesis was carried out using a dual PCR approach, as follows: Two PCR fragments each were

amplified for Roquin (G2623/G2577, G2576/G2579) and Roquin2 (G2556/G2555, G2554/G2622), annealed and used as DNA templates for a second PCR with the outer primer pairs (Roquin, G2623/G2579; Roquin2, G2622/G2556). The secondary PCR fragments spanning the mutations were exchanged with the original sequence by restriction digest and subsequent ligation. *Dra*III was used for pLNCX2-EGFP-Roquin-C419R (p3013), and *Mfe*I/*Bst*XI were used for pLNCX2-EGFP-Roquin2-C416R (p3014).

For pcDNA5/FRT/TO-EGFP (p3083), EGFP was excised as a *Hind*III/*Not*I fragment from pEGFP-N1 (Invitrogen), and cloned into pcDNA5/FRT/TO (Invitrogen). For pcDNA5/FRT/TO-EGFP-Roquin (p3084), EGFP-Roquin was excised as a *Not*I-fragment from pLNCX2-EGFP-Roquin (p2838) and cloned into pcDNA5/FRT/TO. For pcDNA5/FRT/TO-EGFP-Roquin2 (p3085), EGFP-Roquin2 was excised as a *Hind*III/*Eco*RV fragment from pLNCX2-EGFP-Roquin2 (p2985) and inserted into the respective sites of pcDNA5/FRT/TO.

To facilitate cloning of Roquin fusion proteins, the EGFP coding sequence was excised from pLNCX2-EGFP-Roquin (p2838) using *Sal*I and replaced by a PCR-amplified EGFP fragment containing a unique *Age*I site downstream of the EGFP sequence, yielding pLNCX2-EGFPA-Roquin (p3090). For the plasmids encoding the N-terminal portion (N-term) of Roquin (pLNCX2-EGFPA-Roquin-2-441aa; p3124) or the ROQ domain (pLNCX2-EGFPA-Roquin-131-360aa; p3153), the Roquin coding sequence was excised from p3090 as a *Age*I/*Cla*I fragment and replaced with corresponding PCR-amplified inserts coding for N-term (G2788/G2840) or ROQ (G2855/G2856). For pLNCX2-EGFPA-Roquin-442-1130aa (p3125) encoding the Roquin C terminus (C-term), a larger N-terminal portion of Roquin was excised as an *Age*I/*Pml*I fragment from pLNCX2-EGFPA-Roquin (p3090) and replaced by a shorter PCR-amplified fragment (G2842/G2843). pLNCX2-EGFPA-Roquin-S060r (p3101) encoding an siRNA s060 (si-Roquin (B))-resistant version of Roquin was generated using the above described dual PCR approach with primers G2788/G2791, G2789/G2790 and G2788/G2789. The resulting fragment harboring four silent point mutations in the s060 seed sequence were cloned into the *Age*I/*Mfe*I sites of pLNCX2-EGFPA-Roquin (p3090). Flag-tagged Roquin-fusion constructs pCI-neo-Flag-Roquin (p3061), pCI-neo-Flag-Roquin-ΔRING (p3062), and pCI-neo-Flag-Roquin-ΔROQ (p3063) were kindly provided by Nancy Kedersha and Paul Anderson (Harvard Medical School, Boston, MA). Primer sequences are provided in Table S7. Mutations, cloning boundaries and coding sequences in all plasmids were verified by DNA sequencing (GATC Biotech).

mRNA Decay Assay

For mRNA decay experiments, NIH 3T3 B2A2 or HeLa cells were transiently transfected with puroMXβglobin reporter plasmids. 24 hr posttransfection, 5 μg/ml actinomycin D (actD, AppliChem, Cat. No. A1489) was added to the medium for the indicated time intervals before harvesting cells and extracting total RNA using the Genematrix universal RNA purification kit (Eurx, Roboklon). RAW264.7 cells were stimulated for 2 hr with LPS (100 ng/ml) before addition of actD. mRNA half-lives were calculated assuming a first order decay rate. After background subtraction, mRNA signals were normalized to the signal of the loading control and plotted against time. Curves with the following equation were fitted to the data points by linear regression: $y = a \times e^{(b \times t)}$, where y stands for the relative mRNA signal and t for the time. mRNA half-lives were calculated as follows: $t_{1/2} = \ln(2) / \ln(b)$.

In-Line Probing

In-line probing was performed as described previously (Regulski and Breaker, 2008). Mouse TNF-α-CDE RNA was transcribed in vitro using T7 RNA polymerase, dephosphorylated and radiolabelled with [γ-^{32}P]ATP. T7-linkered primers (G2234/G2235, Table S7) were used to amplify the DNA sequence of TNF-α-CDE_{37}-V2 (92 nt) and TNF-α-CDE_{37}-V3 (94 nt) from plasmid templates. For the CDE_{150} DNA template, primers G2332/G2333 and plasmid puroMXß-TNF-α-3′UTR (p2914) containing the full-length 3′UTR of mouse TNF-α were used. After gel-extraction of the DNA templates, RNAs were prepared by in vitro transcription using T7 RNA polymerase (NEB) in a solution containing 40 mM Tris-HCl (pH 7.9 at 25°C), 6 mM $MgCl_2$, 2 mM spermidine, and 10 mM dithiothreitol (DTT). The transcription products were subjected to denaturing 8 M urea/6% polyacrylamide gel electrophoresis (PAGE) for purification. The RNA transcripts were dephosphorylated using calf intestinal phosphatase (Roche) and radiolabeled with [γ-^{32}P]ATP using T4 polynucleotide kinase (NEB) in 70 mM Tris-HCl (pH 7.6 at 25°C), 10 mM $MgCl_2$, 5 mM DTT. The radiolabeled RNA was purified using denaturing 6% PAGE. The purified RNA was subsequently incubated for 45 hr at room temperature in a solution containing 50 mM Tris-HCl (pH 8.3 at 25°C), 20 mM $MgCl_2$, and 100 mM KCl. Reactions were quenched with urea and EDTA prior to loading. Products of spontaneous in-line cleavage were resolved next to a no reaction (NR) control, a partial RNase T1 digest (T1), and a partial alkaline digest ($^{-}$OH) of the same RNA by denaturing 10% PAGE. Gels were dried and visualized using a GE Typhoon laser scanner under the phosphorimager setting.

Northern Blot Analysis

5-15 μg of RNA was resolved by 1.1% agarose/2% formaldehyde/MOPS (morpholine propane sulfonic acid) gel electrophoresis and blotted over night with 8x saline-sodium citrate (SSC) buffer (1x contains 0.15 M NaCl and 0.015 M sodium citrate) onto Hybond-N+ Nylon membranes (Amersham, GE Healthcare). Membranes were hybridized overnight at 55°C with digoxigenin-labeled RNA probes synthesized in vitro using Sp6 polymerase (Fermentas) and DIG RNA labeling mix (Roche). 500 ng RNA probe was diluted in 10 ml hybridization buffer containing 50% formamide, 5x SSC, 5x Denhard's solution, 5 mM EDTA, 10 mM PIPES pH 7.0 at 25°C, 0.4 mg/ml torula yeast RNA (US Biological) and 1% SDS. Membranes were washed twice with 2x SSC/ 0.1% SDS for 5 min, and twice with 0.5x SSC/ 0.1% SDS for 20 min at 65°C. Alkaline phosphatase-coupled anti-digoxigenin Fab fragments and CDP-Star substrate (both Roche) were used for detection according to the manufacturer's instructions. Templates for RNA probes were generated by PCR

using the following primers: G1000/G1001 (probe against exon 1 and 2 of rabbit β-globin), G83/G1009 (probe against human nucleolin), G078/G1008 (probe against mouse S7), and G314/G316 (probe against mouse TNF-α). Deadenylated mRNA was generated using RNase H (NEB) and oligo-dT as described (Sandler et al., 2011). 1.6% agarose gels were used to resolve poly(A) tails, and the corresponding signals were quantified using ImageJ software.

For miRNA detection by northern blot, total RNA was isolated from MEFs with the RNeasy Plus Mini Kit (QIAgen), using 100% ethanol in the RNA binding step. 10 μg RNA was resolved on an 8% urea/15% polyacrylamide gel and transferred onto Hybond-N+ Nylon membranes by semi-dry blotting for 90 min at 25 V. After UV crosslinking and hybridization for 1 hr at 37°C with a miR-16-specific digoxigenin-labeled DNA probe, the membrane was washed twice with 2x SSC/0.1% SDS for 5 min at 37°C, and twice with 0.1x SSC/0.1% SDS for 15 min at room temperature. For detection of U6 snRNA, the membrane was hybridized overnight at 42°C with a U6-specific digoxigenin-labeled DNA probe and washed at 52°C. Probes were generated using the 2nd generation DIG oligonucleotide 3′-end labeling kit (Roche) and the following oligonucleotides: miR-16, 5-CGCCAATATTTACGTGCTGCTA-3′; U6 snRNA, 5′- ATCTTCTCTGTATCGTTCCAATTTTAGTAT-3′.

Quantitative RT-PCR

For RT-qPCR analysis, cDNA was synthesized from 1-2 μg of total RNA using random hexamer primers (Fermentas) and Transcriptor reverse transcriptase (Roche) according to the manufacturer's instructions. PCR reactions were assembled in 384-well plates using 1:20 of a cDNA reaction, 400 nM of each target-specific primer and the DNA SYBR Green I Master kit (Roche) in a final volume of 10 μl per well. qPCR was performed on the Lightcycler 480 system (Roche). Mouse gene-specific primer sequences used for detection of mRNAs encoding nucleolin (G1706/G1707), Ier3 (G1712/G1713), TNF-α (G1844/G1845), Gapdh (G2053/G2054), Nfkbiz (G2181/G2182), Nfkbid (G2199/G2200), NupL1 (G2364/G2365), Roquin (G2392/G2393), Roquin2 (G2394/G2395), Ppp1r10 (G2592/G2593), Bmpr1a (G2723/G2724), Pdia6 (G2729/G2730), Hmgxb3 (G2737/G2738) and Rck (G2747/G2748) are given in Table S7.

Protein IP

HEK293T cells were transiently transfected 24 hr prior to lysis. Cells of a confluent 10-cm dish were washed once with phosphate buffered saline (PBS), collected in a 2 ml reaction tube, and the cell pellet was disrupted mechanically using a tissue lyser (QIAgen TissueLyser II). The lysate was solubilized in 400 μl ice cold RNP lysis buffer (20 mM Tris-HCl (pH 7.5 at 25°C), 100 mM KCl, 1.5 mM $MgCl_2$, 1 mM DTT, 1 tablet/10 ml Mini Complete Protease Inhibitors, EDTA-free (Roche)), and cell debris was removed by centrifugation. 1:20 of the lysate was saved as input before EGFP-tagged proteins were purified using the GFP-binder as described previously (Rothbauer et al., 2008). Lysates were incubated with sepharose-coupled GFP-binder for 1-3 hr at 4°C, followed by two washes with lysis buffer and three to four washes with RNP wash buffer (20 mM Tris-HCl (pH 7.5 at 25°C), 150 mM KCl, 2.5 mM $MgCl_2$, 1 mM DTT). Proteins were eluted from the beads with 1% SDS-containing sample buffer.

RNA IP

Cells grown in 10-cm dishes were mechanically disrupted as described above for protein IP, and solubilized in 400 μl RNA IP lysis buffer (20 mM Tris-HCl (pH 7.5 at 25°C), 150 mM NaCl, 1.5 mM $MgCl_2$, 1 mM DTT, Mini Complete protease inhibitors (Roche), 2 mM vanadylribonucleosid complex RNase inhibitor (NEB) or 0.2 U/ml RNasin (Promega)). 1:13 of the lysate was saved as RNA input, 1:40 for protein input. For IP of EGFP-tagged proteins, lysates were bound to GFP-binder beads for 2-4 hr at 4°C before washing twice with RNA IP lysis buffer and four times with RNA IP wash buffer (20 mM Tris-HCl (pH 7.5 at 25°C), 300 mM NaCl, 2.5 mM $MgCl_2$, 1 mM DTT, 2 mM vanadylribonucleosid complex RNase inhibitor (NEB)). Protein was eluted from 1:5 of the beads using SDS sample buffer; RNA was eluted from 4:5 of the beads using 500 μl TriFast reagent (PeqLab) according to the manufacturer's instructions. 15 μg GlycoBlue (Ambion) was added to the RNA prior to precipitation. For RNA IP of endogenous Roquin from RAW264.7 macrophages, lysates were precleared with Protein A/G UltraLink Resin (Thermo Pierce) for 1 hr at 4°C. 4 μg Roquin antibodies (rabbit polyclonal, Bethyl, 514A and 515A, 2 μg each) or HA control antibody (mouse monoclonal, MMS-101P, Covance Innovative Antibodies) were added for 2 hr at 4°C prior to incubation with protein A/G beads for another 2 hr. Flag IPs were carried out using Flag antibody (M2, F3165, Sigma). For qPCR analysis following RNA IP, a fixed volume of RNA extracted from IP and input samples was used for RT.

Crosslinking RNA IP

The crosslinking protocol was adapted from (Niranjanakumari et al., 2002), as follows. Cells of a confluent 15-cm dish were harvested 24 hr posttransfection, washed twice with PBS and then crosslinked with 0.05% formaldehyde (Merck) in PBS for 10 min at room temperature while rotating. Excess formaldehyde was quenched by addition of 0.25 M glycine (pH 7.0 at 25°C) for 5 min at room temperature. Afterward, cells were washed twice with ice-cold PBS and lysed by mechanical disruption as described above. EGFP-tagged proteins were immunoprecipitated from cytoplasmic lysates using GFP-binder beads as described for RNA IP. Beads were split into equal amounts before washing five times with high stringency RNA IP wash buffer containing either 0 or 4 M urea. 4:5 of the beads were subjected to RNA purification, while 1:5 was used for protein analysis. Before RNA extraction using TriFast (PeqLab), the IP samples were digested with 100 μg/ml proteinase K (Promega) for 30 min at 10°C in a buffer containing 50 mM Tris (pH 7.5 at 25°C), 5 mM $CaCl_2$, 2.5 mM $MgCl_2$ and 4 M urea (pH 7.0 at 25°C). Prior to protein elution with SDS sample buffer, the IP samples were digested with 0.01 ng/ml RNase A (Genomed) in RNA IP wash buffer for 30 min at 4°C.

Mass Spectrometry

Mass spectrometry analysis was carried out at the mass spectrometry and proteomics core facility of the ZMBH (Zentrum für Molekulare Biologie der Universität Heidelberg). Proteins eluted from the RNA affinity or the GFP-binder matrix were shortly run into a 10% polyacrylamide Tris-glycine gel (NuPAGE, Novex/Invitrogen), and proteins were stained by colloidal Coomassie blue. For each sample, the entire lane was cut into three gel slices and processed after in-gel tryptic digestion for LC-MS/MS analysis, as described in more detail previously (Sandler et al., 2011).

Western Blot Analysis

Proteins were resolved on 5%–20% polyacrylamide gradient Tris-glycine gels and transferred onto 0.2 μm pore size nitrocellulose membranes (Peqlab). Membranes were then blocked in PBS containing 0.1% sodium azide and 5% horse serum or milk powder, incubated with antibodies diluted in the same solution, and washed in 150 mM NaCl, 50 mM Tris-HCl (pH 7.5 at 25°C), 1% Tween-20. Horseradish peroxidase-coupled secondary antibodies (Jackson Immunoresearch) in combination with Western Lightning enhanced chemiluminescence substrate (Perkin Elmer) were used for detection. For Dicer expression analysis, MEFs were directly lysed in 10 mM Tris-HCl (pH 7.5 at 25°C), 150 mM NaCl, 1.5 mM $MgCl_2$ and 0.65% NP-40. Nuclei were removed by centrifugation. For the detection of Roquin and TNF-α in RAW264.7 macrophages, cells were harvested, washed once in PBS, solubilized in RNA IP lysis buffer, and cytoplasmic lysates were supplemented with SDS sample buffer prior to western blot analysis.

Antibodies

The following primary antibodies were used for western blot analysis: mouse monoclonal anti-G3BP1 (TT-Y, sc-81940, Santa Cruz), anti-HuR (3A2, sc-5261, Santa Cruz), anti-Flag (M2, F3165, Sigma) and anti-GFP (Roche); rabbit polyclonal anti-cNot1 (14276-1-AP, Proteintech), anti-GFP (ab290, Abcam), anti-p54/Rck (A300-443A, Bethyl Laboratories), and anti-Roquin (514A and 515A, Bethyl); goat polyclonal anti-TNF-α (sc-1351, Santa Cruz); and rat monoclonal antibody against α-tubulin (ab6160, Abcam). Polyclonal rabbit anti-Dicer antibody (#349) was kindly provided by Witold Filipowicz (Friedrich Miescher Institute for Biomedical Research, Basel, Switzerland), and polyclonal rabbit anti-Caf1a antibody was kindly provided by Ann-Bin Shyu (University of Texas-Houston Medical School).

EMSA

To express a recombinant N-terminal His-tagged fragment of Roquin (aa 2-440, Roquin-N), plasmid pETM11-Roquin-N (p2940, a kind gift of Vigo Heissmeyer, Helmholtz Center Munich, Germany) was transformed into BL21 codon+ *E. coli* cells. Cells were cultured in LB medium at 37°C to an OD_{600} of 0.5, and protein expression was induced by addition of 1 mM IPTG. The culture was then incubated for additional 16 hr at 21°C before cells were lysed using a microfluidizer (Emulsiflex, Avestin). The recombinant protein was purified on Ni-Sepharose 6FastFlow beads (GE-Healthcare) under nondenaturing conditions and eluted in elution buffer (20 mM Tris-HCl (pH 8.0 at 25°C), 1 mM $MgCl_2$, 200 mM NaCl, 270 mM imidazole (pH 8.0 at 25°C), 0.1% NP-40, 10% glycerol, 1 tablet/10 ml Mini Complete Protease Inhibitors, EDTA-free (Roche)).

The EMSA was performed according to Ryder et al. (2008) with the following modifications: RNA was prepared by 5′ end-labeling 200 pmol of commercially synthesized RNA oligonucleotides (23 nt, Biomers.net, Germany) with [γ-^{32}P]-ATP using T4 polynucleotide kinase (NEB) as described above for in-line probing. Labeled RNA was separated from unincorporated nucleotides by column purification (QIAquick Nucleotide Removal Kit, QIAgen) and adjusted with H_2O to 1 pmol/μl. Prior to binding reactions, a mastermix containing 500 pM labeled RNA (10 fmol per 20 μl reaction), 1x binding buffer (20 mM Tris-HCl (pH 7.5 at 25°C), 50 mM KCl, 5 mM $MgCl_2$, 20 μM $ZnSO_4$, 10% glycerol), 2 mM DTT, 0.1 mg/ml BSA, 3.75 μg/ml tRNA and 5 μg/ml heparin was heated at 55°C for 3 min and cooled down at room temperature for 5 min to promote RNA folding. In parallel, a dilution series of 10x protein stocks was prepared in 1x protein dilution buffer (1x binding buffer, 5 μg/ml heparin, 0.2 U/ml RNasin (Promega), 1 tablet/10 ml Mini Complete Protease Inhibitors, EDTA-free (Roche)). For each binding reaction, 2 μl of the 10x protein stock was added to 18 μl of the mastermix at room temperature for 10 min. Reactions were then supplemented with 4 μl of 6x loading buffer (30% glycerol, bromphenol blue, xylene cyanol) and placed on ice. RNP complexes were resolved by nondenaturing PAGE (6% polyacrylamide, 0.5x TBE, 20 μM $ZnSO_4$, 5% glycerol) in ice-cold 0.5x TBE buffer (2 mM EDTA, 20 μM $ZnSO_4$) at 200 V for 40 min at 4°C. Gels were dried and exposed to a phosphor imager screen.

To calculate the K_d, the fraction of Roquin-N-bound RNA (specific binding, *y* variable) was plotted against the initial concentration of Roquin-N (*x* variable). Using Graphpad Prism software, a curve with the following equation was fitted to the data points: $y = y_{max}^{\ h} \times x^h / (K_d^{\ h} + x^h)$, whereby y_{max} is the maximum specific binding, K_d the dissociation constant, and h the Hill coefficient.

Knockdown by siRNA

NIH 3T3 B2A2 cells were transfected twice with siRNAs at a final concentration of 100 nM over a time period of four days using Lipofectamine RNAiMAX (Invitrogen) and OptiMEM (GIBCO) according to the manufacturer's instructions. The second siRNA transfection on the third day included plasmid DNA. For rescue experiments, NIH 3T3 cells were transfected with siRNAs on the first day, plasmids were transfected using PEI on the second day, and the mRNA decay assay was performed on the third day. RAW264.7 macrophages were transfected twice on two consecutive days with siRNAs at a final concentration of 100 nM over a time period of three days using Lipofectamine LTX (Invitrogen) and OptiMEM (GIBCO) according to the manufacturer's instructions. Mouse

siRNAs used in this study were synthesized by Eurofins MWG Operon. They correspond to the following sequences (sense strand): D0 (s015, control), 5′-GCAUUCACUUGGAUAGUAAdTdT-3′; C2 (s014, control), 5′-GCAUUCACUUGGAUAGUAAdTdT-3′; Roquin (A) (s051), 5′-CCUUCUAUCUGCUGAAAGAdTdT-3′; Roquin (B) (s060), 5′-CGCACAGTTACAGAGCTCAdTdT-3′; Roquin2 (s055), 5′-GGACTTGGCTCATAAATCAdTdT-3′.

ELISA

After kd of Roquin in RAW264.7 macrophages, supernatants were collected from cells exposed to LPS (100 ng/ml) for different periods of time, and the concentration of secreted TNF-α was measured using the murine TNF-α ELISA development kit (PeproTech, 900-K54) according to the manufacturer's instructions. TNF-α concentrations were normalized to the amount of total RNA extracted from the same cells, and the resulting ratio was expressed as arbitrary units (A.U.).

EGFP-Roquin Affinity Purification

HEK293 cell lines stably expressing EGFP, EGFP-Roquin or EGFP-Roquin2 in a tetracycline-inducible manner were generated using the Flp-In T-REx Core Kit (Invitrogen, K6500-01). pcDNA5/FRT/TO-EGFP (p3083), pcDNA5/FRT/TO-EGFP-Roquin (p3084) and pcDNA5/FRT/TO-EGFP-Roquin2 (p3085) together with pOG44 expressing Flp recombinase were transfected in a 1:9 ratio into HEK293 T-REx Flp-In-293 cells. Stable transfectants were selected with hygromycin B (125 μg/ml), and individual clones were tested for protein expression after induction with doxycyclin (1 μg/ml) by western blot analysis using α-GFP antibody.

For protein purification, cells were grown to confluency in 15-cm dishes (5 dishes for EGFP, 10 for EGFP-Roquin, and 15 for EGFP-Roquin2) and protein expression was induced with 1 μg/ml doxycyclin 24 hr prior to lysis. Cells were collected, washed once with PBS and resuspended in 1–4 ml hypotonic buffer (100 mM HEPES (pH 7.5 at 25°C), 10 mM KCl, 1.5 mM $MgCl_2$, 0.5 mM DTT, 1 tablet/10 ml Mini Complete Protease Inhibitors, EDTA-free (Roche)). Following 15 min incubation on ice, cells were lysed mechanically by repeated passage through a 0.5 mm needle. Cell debris was removed by centrifugation. To enrich for EGFP-Roquin and EGFP-Roquin2, the corresponding lysates were subjected to ultracentrifugation (100,000 × g for 30 min), and the pellets were resuspended in 1 ml IP buffer (100 mM HEPES (pH 7.5 at 25°C), 100 mM KCl, 50 mM NaCl, 1.5 mM $MgCl_2$, 0.5 mM DTT, 1 tablet/10 ml Mini Complete Protease Inhibitors, EDTA-free (Roche)). The lysate of EGFP-expressing cells was adjusted to equal salt concentrations by addition of KCl and NaCl without ultracentrifugation. EGFP-tagged proteins were purified using the GFP-binder as described previously (Rothbauer et al., 2008). Lysates were incubated with sepharose-coupled GFP-binder for 1–3 hr at 4°C, followed by two washes with lysis buffer and 3–4 washes with IP wash buffer (100 mM HEPES (pH 7.5 at 25°C), 150 mM KCl, 50 mM NaCl, 2.5 mM $MgCl_2$, 0.5 mM DTT, 1 tablet/10 ml Mini Complete Protease Inhibitors, EDTA-free (Roche)). Proteins were eluted from the beads with SDS-containing sample buffer (50 mM HEPES (pH 7.5 at 25°C), 2% SDS, 1 tablet/10 ml Mini Complete Protease Inhibitors, EDTA-free (Roche)). Efficiency of the IP was verified by western blot analysis using 5% of the eluates; 50% of the eluates was subjected to mass spectrometry.

Morpholino Delivery

For delivery of antisense morpholino oligonucleotides, RAW264.7 cells or BMDM were seeded into 12-well plates one and 10-12 days prior to transfection, respectively. Morpholinos were stored at 4°C (−20°C for long term storage) and heated at 65°C for 5 min before use. Morpholinos were added to the medium at a final concentration of 2 μM in the presence of 6 μM Endo-Porter (Gene Tools, LLC) according to the manufacturer's protocol. 24 hr later, cells were stimulated with LPS (100 ng/ml) for 6 hr. Cells were washed with PBS and either collected by trypsinization for lysis (RAW264.7) or lysed directly on the dish (BMDM) for total RNA extraction using the Genematrix universal RNA purification kit (Eurx, Roboklon). For RNA IP, HEK293T cells were transfected with 2 μM morpholino and plasmid simultaneously using Lipofectamine 2000 (Life Technologies) according to the manufacturer's protocol.

The following 25-mer morpholinos were obtained from Gene Tools, LLC: CDE-MO-1 targeting the left arm of the TNF-α CDE (m001), 5′-GAAAACATGTCTGTCTGAAGACAGC-3′; CDE-MO-2 targeting the right arm of the TNF-α CDE (m002), 5′-GGACAGCT CAGCTCCGTTTTCACAG-3′; UTR-MO targeting a TNF-α 3′UTR sequence downstream of the CDE (m003), 5′-AGCCTGGTCAC CAAATCAGCGTTAT-3′; and Ctrl-MO as the standard control oligo from Gene Tools (m004), 5′-CCTCTTACCTCAGTTACAATT TATA-3′.

Data Sources for Sequence Alignments

For sequence conservation analysis of TNF-α and ICOS CDEs, GenBank mRNA 3′UTR sequences were retrieved for different species from the National Center for Biotechnology Information (NCBI) database: TNF-α: mouse (*Mus musculus*; accession number NM_013693), human (*Homo sapiens*; NM_000594), chimpanzee (*Pan troglodytes*; XM_001152827), orangutan (*Pongo abelii*; XM_002816720), macaque (*Macaca mulatta*; NM_001047149), swine (*Sus scrofa*; NM_214022), zebu (*Bos indicus*; AF011927), cow (*Bos taurus*; NM_173966), goat (*Capra hircus*; X14828), sheep (*Ovis aries*; NM_001024860), dog (*Canis lupus familiaris*; NM_001003244), horse (*Equus caballus;* NM_001081819), giant panda (*Ailuropoda melanoleuca*; XM_002930032), rabbit (*Oryctolagus cuniculus*; NM_001082263), african elephant (*Loxodonta africana*; XM_003422213), rat (*Rattus norvegicus*; NM_012675), marmot (*Marmota monax*; AF096268), guinea pig (*Cavia porcellus*; NM_001173025), and chinese hamster (*Cricetulus griseus*; XM_003508487); ICOS: mouse (*Mus musculus*; NM_017480), human (*Homo sapiens*; NM_012092), chimpanzee (*Pan troglodytes*;

XM_001173460), orangutan (*Pongo abelii*; XM_002812772), macaque (*Macaca mulatta*; XM_001104581), swine (*Sus scrofa*; NM_001044546), and cow (*Bos taurus*; NM_001034275). CDE sequence conservation analysis of Nfkbid, Nfkbiz, Ier3, Roquin, Roquin2, Bmpr1a, Pdia6, Ppp1r10 and Hmgxb3 was based on sequences retrieved from the UCSC whole-genome alignment of 46 vertebrate organisms (Fujita et al., 2011).

For conservation analysis of Roquin, we retrieved the following protein sequences from NCBI and aligned them by ClustalW: mouse (*Mus musculus*; NP_001020123.1), chicken (*Gallus gallus*; XP_001234605.2), African clawed frog (*Xenopus laevis*; NP_001084548.1), zebrafish (*Danio rerio*, NP_001108155.1), lancelet (*Branchiostoma floridae*; XP_002588179.1), sea squirt (*Ciona intestinalis*; XP_002125601.1), sea urchin (*Strongylocentrotus purpuratus*; XP_780349.3), red flour beetle (*Tribolium castaneum*; EFA08769.1), fruit fly (*Drosophila melanogaster*; NP_648886.1), water flea (*Daphnia pulex*; EFX88973.1), tick (*Ixodes scapularis*; XP_002414149.1), roundworm (*Ascaris suum*; ADY40466.1; *Caenorhabditis elegans*, CCD31104.1), sea anemone (*Nematostella vectensis*, XP_001626669.1), hydra (*Hydra magnipapillata*; XP_002158024.1), and sponge (*Amphimedon queenslandica*; XP_003385928.1).

Bioinformatics Prediction of CDEs

CDEs in the mouse transcriptome were predicted with in house developed R scripts. Sequences of all RefSeq mRNAs were downloaded from NCBI on December 8, 2011, as a FASTA file and read by R with the R package seqinR (Charif and Lobry, 2007). Coding sequence positions and GeneIDs were extracted from the Feature Table. With a 21 nt sliding window, 3′UTRs were searched for stem-loops that are similar to the TNF-α CDE according to the following criteria: A stem of at least 5 canonical base-pairs, with 5′-TTC-3′/5′-GAA-3′ in the apical part, separated by a pyrimidine-purine-pyrimidine loop (see consensus motif in Figure 6A). An extension of the stem to 9 canonical base-pairs, or 8 canonical base-pairs and a G-U wobble, were not allowed because a cloning context that provides such an extension inactivated the CDE (TNF-α-CDE$_{17}$-ds, Figure 2D).

To investigate conservation of the identified sequences in the UCSC 46 vertebrate genome alignment (Fujita et al., 2011), their genomic coordinates were determined by combining the coordinates of putative CDE-containing mouse genes in the UCSC Genes and Gene Prediction Track with the results of a BLAT search. MAF blocks that overlap the putative mouse CDEs and 5 additional nucleotides upstream and downstream were retrieved through Galaxy (Blankenberg et al., 2011). Since the sequence of the CDE in the basal part of the stem and its context is highly flexible, it was important to avoid that small insertions or deletions relative to the mouse CDE would conceal the presence of a CDE in the aligning species. For each species, the nucleotide that aligns to the center of the mouse CDE loop in the highest scoring MAF block was extracted together with 10 nucleotides upstream and downstream of this genomic coordinate, irrespective of their position in the alignment. The resulting 21 nucleotides were tested according to the CDE criteria mentioned above.

RNA IP, Library Preparation, Deep Sequencing, and Data Analysis

Endogenous Roquin was immunoprecipitated from lysates of RAW246.7 macrophages that had been grown in two 15-cm dishes and stimulated for 2 hr with LPS (100 ng/ml). Beads alone served as control IP. The IP was performed as described in the RNA IP section. RNA was then extracted from both the IP and input samples using TriFast (PeqLab). Library preparation was carried out with Illumina protocols using the service of the BioQuant Deep Sequencing Core Facility at the University of Heidelberg. In brief, 50-100 ng RNA was ethanol-precipitated and resuspended in 19.5 μl Elution, Fragmentation and Prime buffer of the TruSeq mRNA preparation kit (Illumina). The samples were fragmented for 4 min at 94°C, and the standard TruSeq mRNA protocol was applied with the following changes: column purification instead of bead purification, and size selection using a 2% Size Select E-Gel (Invitrogen). Sequencing was performed at the EMBL Genomics Core Facility, Heidelberg, on the Illumina HiSeq2000 instrument, which yielded a raw read length of 58 bases (52 bases for the fragment plus 6 bases for the barcode). Reads were aligned to the *Mus musculus* genome (NCBI build 37) using Burrows-Wheeler Alignment (Li and Durbin, 2009). For data analysis exon coordinates of RefSeq annotated RNAs were retrieved from the UCSC mm9 refGene table (Fujita et al., 2011). mRNAs that had been aligned more than once to the genome in the UCSC genome browser were removed. Reads were summarized for gene models with the Bioconductor package easyRNASeq (Delhomme et al., 2012) and differential expression was tested for with the DESeq package (Anders and Huber, 2010).

Statistical Procedures

GO term enrichment was analyzed with GO::TermFinder (Boyle et al., 2004) for the 55 genes that showed conservation of their CDE-like motifs in at least 10 species (observed frequency). All mouse genes that were initially searched for putative CDEs were used as a background population (expected frequency). The cut-off was set to a Bonferroni-adjusted p value of 0.01.

RNA-seq counts of the Roquin IP were tested for enrichment of transcripts compared to the control IP with the Bioconductor package DESeq (Anders and Huber, 2010). Since sampling error is not the only source of variance in RNA-Seq experiments, DESeq uses the negative binomial distribution as a model. This distribution has one parameter more than the Poisson distribution and can therefore be used to account for sample-to-sample variance beyond the sampling error. The dependence of variation on the mean is estimated from the data and used to compute p values. The Benjamini-Hochberg procedure is used to adjust for multiple testing (Table S6).

To test for enrichment of CDE-containing transcripts among the Roquin targets identified in the Roquin IP (Figure 6B), we used the hypergeometric distribution, which represents the probability of drawing k successes in n draws without replacement from a finite

population of size N that contains K successes. In our case, the hypergeometric p value gives the probability of counting at least the observed number of CDE-containing transcripts by randomly drawing 95 genes (the number of Roquin targets in the Roquin IP) from a population of 13,759 genes (all RefSeq annotated coding genes in the analysis) with a specific number of CDE mRNAs (e.g., 49 for conserved 3′UTR CDEs).

SUPPLEMENTAL REFERENCES

Anders, S., and Huber, W. (2010). Differential expression analysis for sequence count data. Genome Biol. *11*, R106.

Blankenberg, D., Taylor, J., and Nekrutenko, A.; Galaxy Team. (2011). Making whole genome multiple alignments usable for biologists. Bioinformatics *27*, 2426–2428.

Boyle, E.I., Weng, S., Gollub, J., Jin, H., Botstein, D., Cherry, J.M., and Sherlock, G. (2004). GO:TermFinder—open source software for accessing Gene Ontology information and finding significantly enriched Gene Ontology terms associated with a list of genes. Bioinformatics *20*, 3710–3715.

Charif, D., and Lobry, J.R. (2007). SeqinR 1.0-2: a contributed package to the R project for statistical computing devoted to biological sequences retrieval and analysis. In Structural Approaches to Sequence Evolution: Molecules, Networks, Populations (Biological and Medical Physics, Biomedical Engineering), U. Bastolla, M. Porto, H.E. Roman, and M. Vendruscolo, eds. (Berlin, Heidelberg, Germany: Springer Verlag), pp. 207–232.

Delhomme, N., Padioleau, I., Furlong, E.E., and Steinmetz, L.M. (2012). easyRNASeq: a bioconductor package for processing RNA-Seq data. Bioinformatics *28*, 2532–2533.

Fujita, P.A., Rhead, B., Zweig, A.S., Hinrichs, A.S., Karolchik, D., Cline, M.S., Goldman, M., Barber, G.P., Clawson, H., Coelho, A., et al. (2011). The UCSC Genome Browser database: update 2011. Nucleic Acids Res. *39*(Database issue), D876–D882.

Li, H., and Durbin, R. (2009). Fast and accurate short read alignment with Burrows-Wheeler transform. Bioinformatics *25*, 1754–1760.

Niranjanakumari, S., Lasda, E., Brazas, R., and Garcia-Blanco, M.A. (2002). Reversible cross-linking combined with immunoprecipitation to study RNA-protein interactions in vivo. Methods *26*, 182–190.

Ozgur, S., Chekulaeva, M., and Stoecklin, G. (2010). Human Pat1b connects deadenylation with mRNA decapping and controls the assembly of processing bodies. Mol. Cell. Biol. *30*, 4308–4323.

Regulski, E.E., and Breaker, R.R. (2008). In-line probing analysis of riboswitches. Methods Mol. Biol. *419*, 53–67.

Rothbauer, U., Zolghadr, K., Muyldermans, S., Schepers, A., Cardoso, M.C., and Leonhardt, H. (2008). A versatile nanotrap for biochemical and functional studies with fluorescent fusion proteins. Mol. Cell. Proteomics *7*, 282–289.

Ryder, S.P., Recht, M.I., and Williamson, J.R. (2008). Quantitative analysis of protein-RNA interactions by gel mobility shift. Methods Mol. Biol. *488*, 99–115.

Stoecklin, G., Stoeckle, P., Lu, M., Muehlemann, O., and Moroni, C. (2001). Cellular mutants define a common mRNA degradation pathway targeting cytokine AU-rich elements. RNA *7*, 1578–1588.

Stoecklin, G., Gross, B., Ming, X.F., and Moroni, C. (2003). A novel mechanism of tumor suppression by destabilizing AU-rich growth factor mRNA. Oncogene *22*, 3554–3561.

Stoecklin, G., Tenenbaum, S.A., Mayo, T., Chittur, S.V., George, A.D., Baroni, T.E., Blackshear, P.J., and Anderson, P. (2008). Genome-wide analysis identifies interleukin-10 mRNA as target of tristetraprolin. J. Biol. Chem. *283*, 11689–11699.

Winkler, G.S., Mulder, K.W., Bardwell, V.J., Kalkhoven, E., and Timmers, H.T. (2006). Human Ccr4-Not complex is a ligand-dependent repressor of nuclear receptor-mediated transcription. EMBO J. *25*, 3089–3099.

Xu, N., Loflin, P., Chen, C.Y., and Shyu, A.B. (1998). A broader role for AU-rich element-mediated mRNA turnover revealed by a new transcriptional pulse strategy. Nucleic Acids Res. *26*, 558–565.

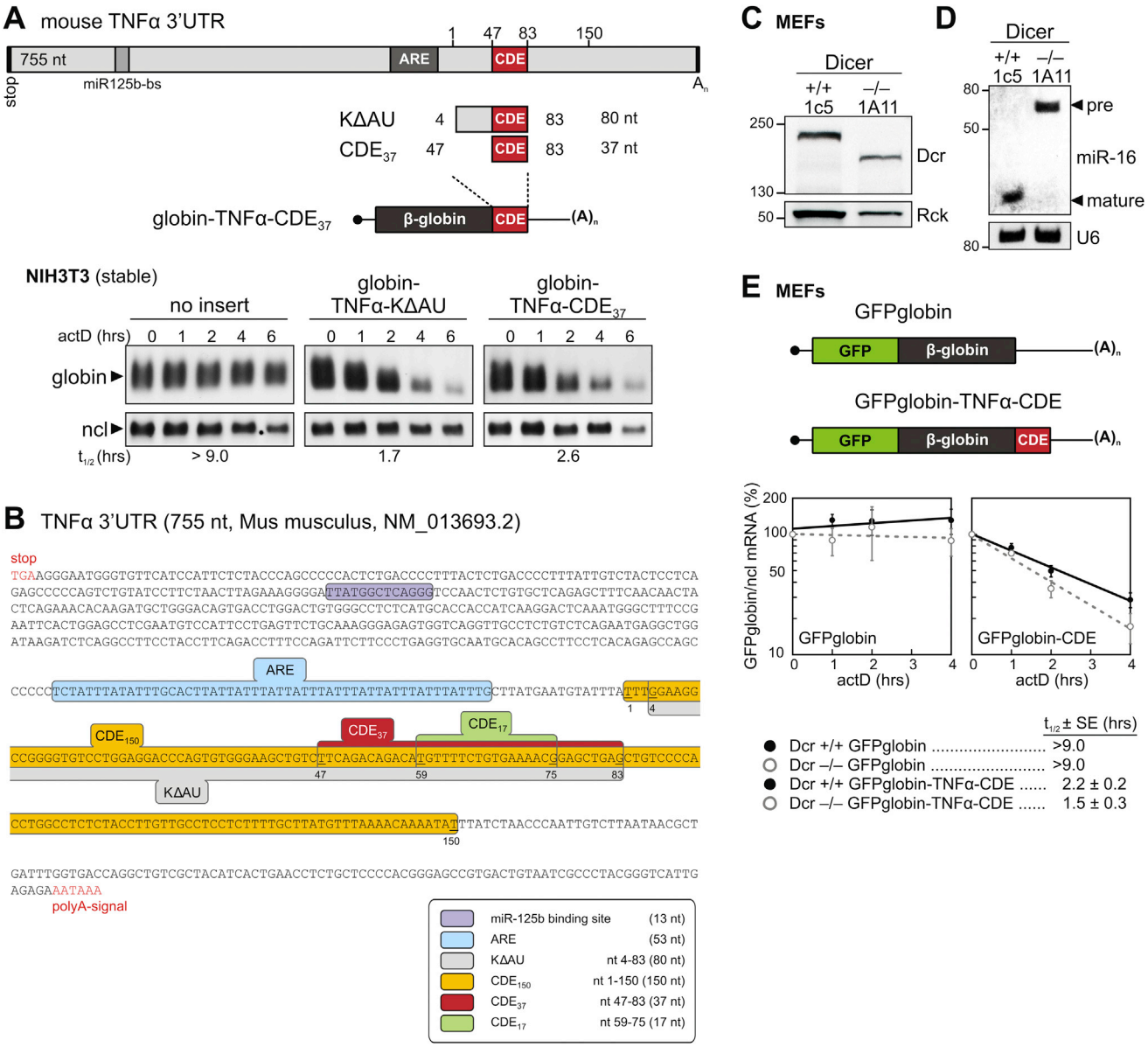

Figure S1. Mapping of the Mouse TNF-α CDE and Dicer-Independent mRNA Decay, Related to Figure 1

(A) Schematic representation of the mouse TNF-α 3′UTR. CDE-containing TNF-α sequences were inserted into the 3′UTR of a globin reporter gene, as depicted. Reporter genes were stably transfected into NIH 3T3 cells, and degradation of the reporter mRNAs was measured upon treatment with 5 μg/ml actinomycin D (actD). Total RNA was extracted at regular time intervals, resolved on 1.1% agarose gels, and subjected to northern blot analysis. Globin mRNA signals normalized to nucleolin (ncl) mRNA were used for calculation of average mRNA half-lives ($t_{1/2}$), n = 2.

(B) Sequence of the mouse TNF-α 3′UTR (755 nt). The miR-125b binding site is marked in purple, the ARE in blue, the CDE_{150} sequence in yellow, the KΔAU fragment in gray, the CDE_{37} in red, and the minimal CDE_{17} stem-loop in green. The stop-codon and the poly(A)-signal are highlighted in red. Nucleotides are numbered according to the CDE_{150} fragment (nt 1-150).

(C) Dicer expression in WT Dicer +/+ MEFs (clone 1c5) and Dicer –/– MEFs (clone 1A11) was analyzed by western blot. Dicer migrates at a lower position in the –/– MEFs due to deletion of exons 22 and 23 comprising the RNase III domain. Rck serves as loading control.

(D) Processing of miR-16 was analyzed by urea-PAGE and northern blot analysis, U6 snRNA serves as loading control. Dicer –/– MEFs (clone 1A11) lack mature miR-16 and accumulate pre-miR-16.

(E) A GFPglobin reporter gene containing the TNF-α CDE in its 3′UTR was stably transfected into Dicer +/+ and –/– MEFs. After treatment with 5 μg/ml actD, reporter mRNA levels were measured by RT-qPCR, normalized to ncl mRNA, plotted as percentage of the initial time point against time (average ± SE, n ≥ 3), and used for calculating reporter mRNA half-lives.

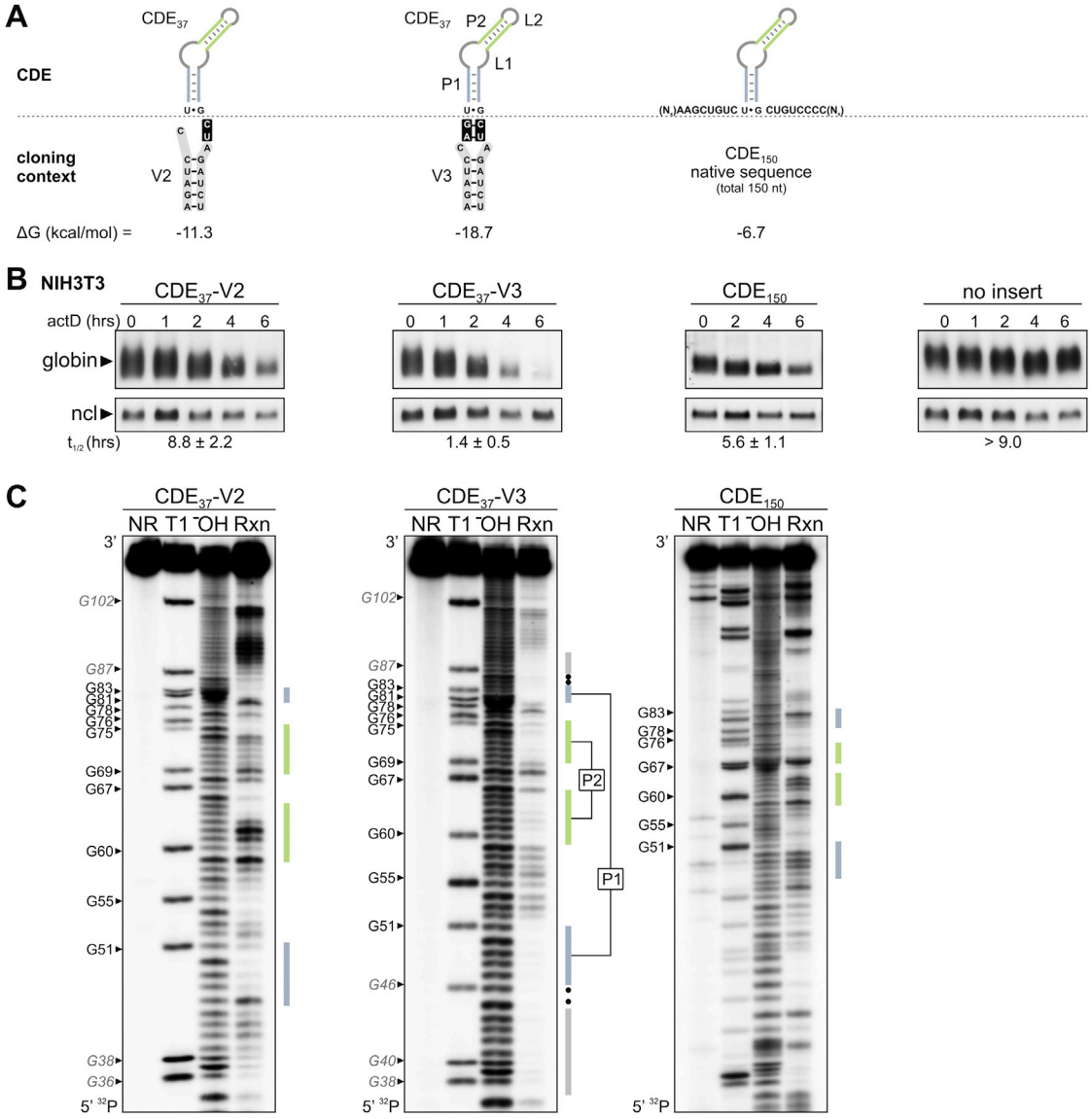

Figure S2. Secondary Structure Comparison of TNF-α CDE Variants, Related to Figure 1

(A) Schematic representation of mouse TNF-α CDE_{37} variants V2 and V3, which differ only in the cloning context, and CDE_{150} spanning a 150 nt region of the mouse TNF-α 3′UTR. The gain in free energy, ΔG, was calculated for the proposed structures at 37°C using Mfold version 3.5.

(B) Globin reporter genes containing TNF-α CDE_{37} variants V2 and V3, CDE_{150} and a control globin reporter lacking an insert were transiently transfected into NIH 3T3 cells. Reporter mRNA degradation was measured as described for Figure 1E. mRNA half-lives are given as average values ± SD, n ≥ 3.

(C) In-line probing analysis of in vitro synthesized, 5′-^{32}P-labeled CDE_{37}-V2, CDE_{37}-V3 and CDE_{150} RNAs. The RNAs were either loaded directly (NR, no reaction), subjected to cleavage by RNase T1 or alkaline hydrolysis (¯OH), or incubated for 45 hr at room temperature and pH 8.3 (in-line reaction, Rxn) prior to urea-PAGE. The in-line of CDE_{37}-V3 (middle panel) is the same as in Figure 1B, shown here again for comparison.

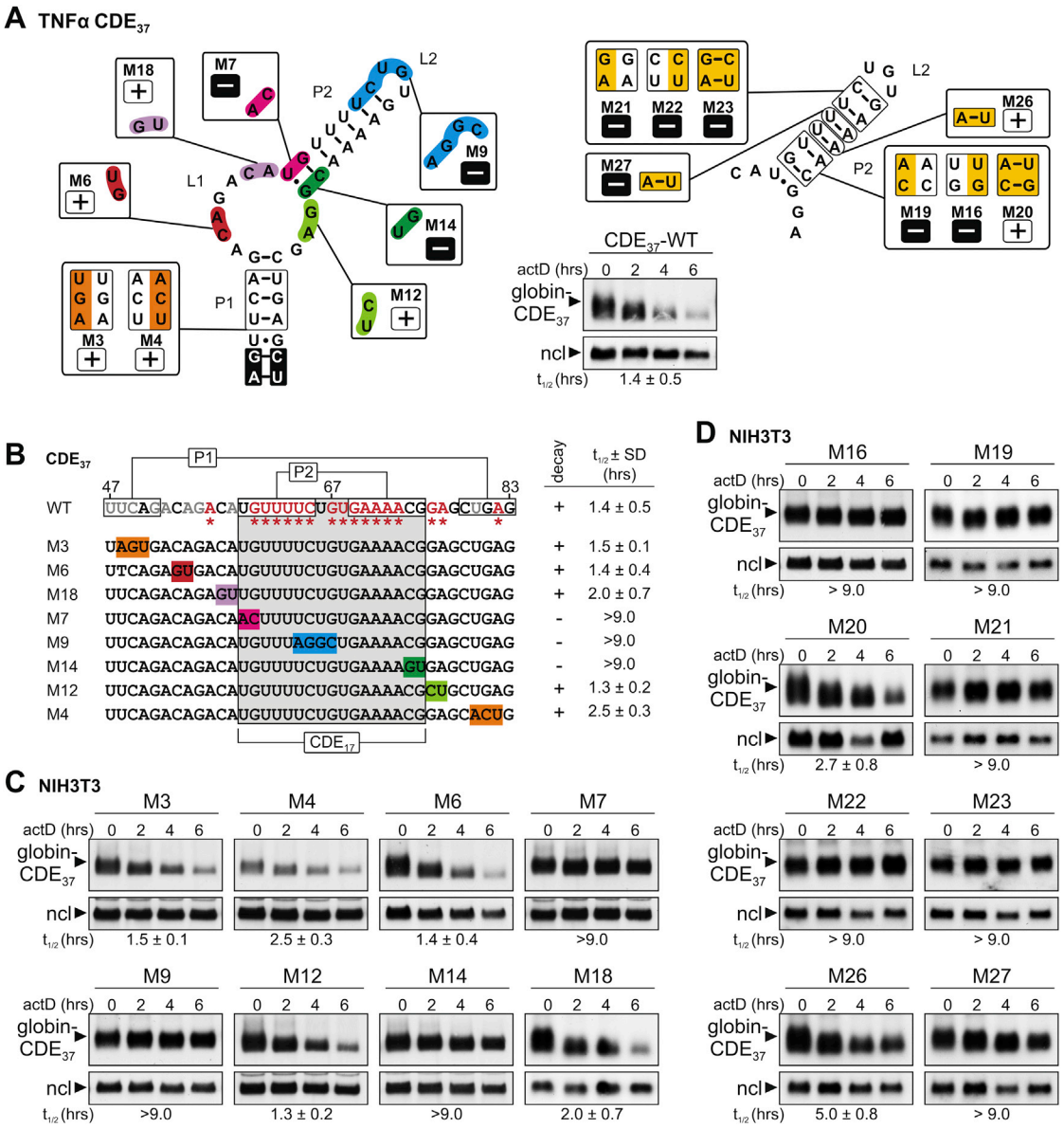

Figure S3. Mutational Analysis of the Mouse TNF-α CDE, Related to Figures 1 and 2

(A) Schematic representation of substitution mutations mapped onto the TNF-α CDE structure. CDE_{37} mutants active in mRNA decay ($t_{1/2}$ < 6.0 hr) are labeled "+," inactive mutants ($t_{1/2}$ > 9.0 hr) are labeled "–." For comparison, decay of globin-CDE_{37}-WT-V3 was measured in transiently transfected NIH 3T3 cells as in Figure 1E.

(B) The same substitution mutations as in the left panel of (A) were mapped onto the linear TNF-α CDE sequence, together with $t_{1/2}$ ± SD ($n \geq 3$) of the corresponding reporter mRNAs.

(C) The effect of the CDE_{37} substitution mutations (in the V3 cloning context) on mRNA degradation was measured by transiently transfecting NIH 3T3 cells with the corresponding globin reporter genes. Northern blot analysis was carried out as in Figure 1E, average $t_{1/2}$ ± SD, $n \geq 3$.

(D) P2 stem mutations were introduced into the TNF-α CDE_{37}-V3, either in one strand to disrupt P2, or as compensatory mutations in both strands to restore P2. Globin reporter mRNA decay was measured in transiently transfected NIH 3T3 cells by northern blot analysis as in Figure 1E, average $t_{1/2}$ ± SD, $n \geq 3$.

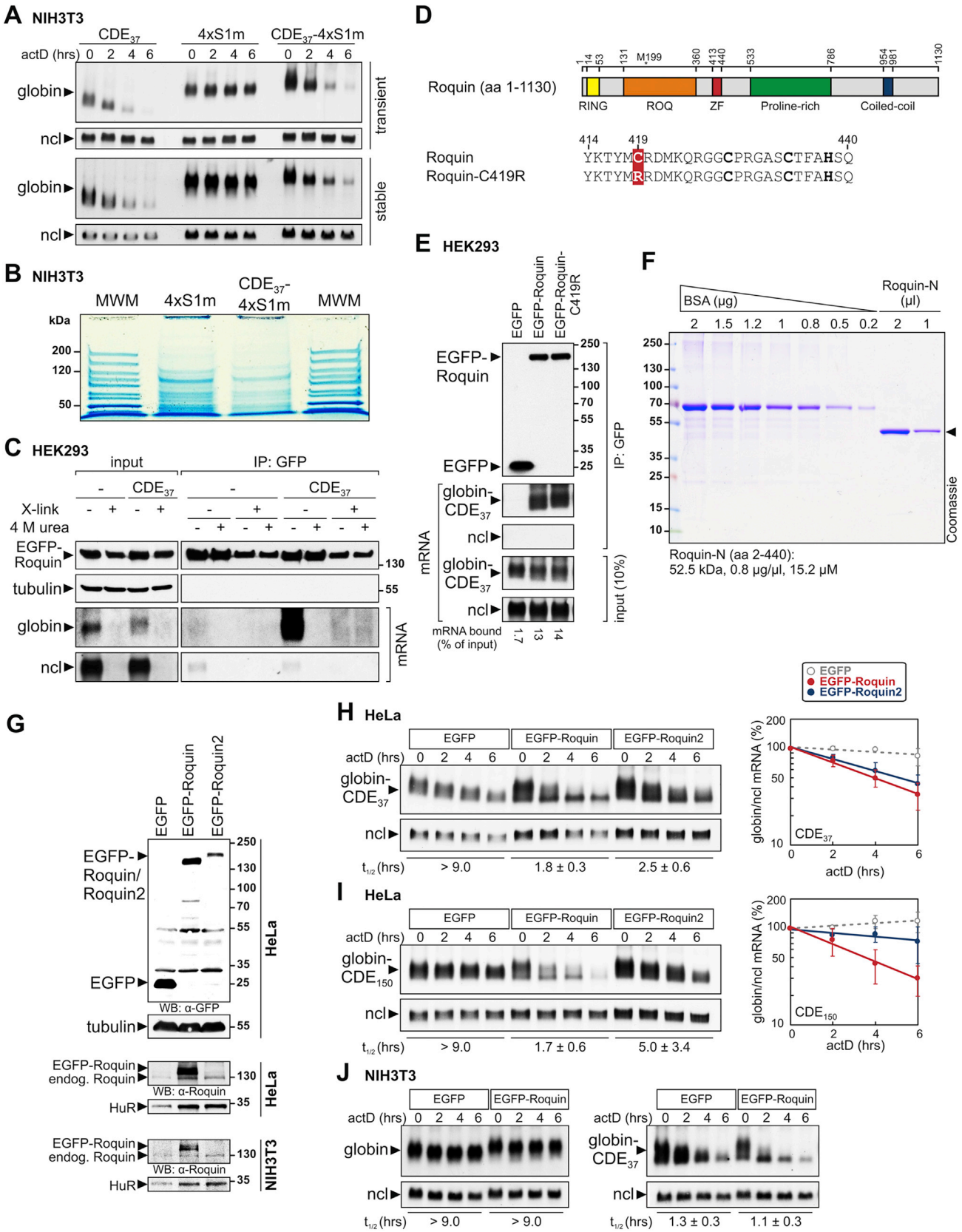

(legend on next page)

Figure S4. Purification and Activity of Roquin/Roquin2, Related to Figures 3 and 4

(A) NIH 3T3 cells were transfected transiently (upper panel) and stably (lower panel) with globin reporter genes containing in their 3′UTR either the TNF-α CDE_{37}, an improved streptavidin-binding aptamer 4xS1m, or both. Reporter mRNA degradation was monitored by northern blot analysis as in Figure 1E.

(B) For purification of CDE-binding proteins, RNAs containing the 4xS1m alone or CDE_{37}-4xS1m were synthesized in vitro, coupled to streptavidin sepharose beads, and incubated with cytoplasmic lysates of NIH 3T3 cells. After washing, proteins were eluted from the affinity matrix using RNase A, resolved by PAGE and visualized by colloidal coomassie blue staining. MWM, molecular weight marker.

(C) Binding of Roquin to the globin-TNF-α-CDE_{37} mRNA was analyzed by RNA IP after crosslinking. This is a repeat experiment to Figure 3B and contains the globin reporter mRNA lacking a CDE as an additional negative control.

(D) Schematic representation of mouse Roquin domains; ZF, zinc finger. The sequence shows the ZF disrupting mutation C419R. Numbers refer to amino acid positions.

(E) HEK293 cells were transiently transfected with globin-TNF-α-CDE_{37}-V3 together with either EGFP, EGFP-Roquin or EGFP-Roquin-C419R. After IP of the EGFP-tagged proteins, the globin reporter mRNA was visualized by northern blot analysis, ncl mRNA serves as a negative control for unspecific binding. The fraction of mRNA bound by IP is given as percentage of the input.

(F) Roquin-N (amino acids 2–440) was expressed as a His-tagged protein in *E. coli* and purified via nickel-sepharose beads. To determine its purity and concentration, the protein was resolved by SDS-PAGE next to a dilution series of bovine serum albumin (BSA), and stained with Coomassie blue.

(G) Equal amounts of plasmid encoding EGFP, EGFP-Roquin or EGFP-Roquin2 were transiently transfected into HeLa cells, corresponding to the amounts used for the experiments in Figures S7B and S7C. In the upper panel, proteins were detected by anti-GFP western blot analysis, tubulin serves as a loading control. In the middle panel, endogenous Roquin and EGFP-Roquin were detected using an anti-Roquin antibody, HuR serves as a loading control. In the bottom panel, the same analysis was carried out in transiently transfected NIH 3T3 cells.

(H) HeLa cells were transiently transfected with EGFP, EGFP-Roquin or EGFP-Roquin2 together with globin-TNF-α-CDE_{37}-V3. Left panel, degradation of the reporter mRNA was measured as in Figure 1E, average $t_{1/2} \pm$ SD, $n \geq 3$. Right panel, decay curves show average globin reporter mRNA levels normalized to ncl mRNA as percentage of the initial value (±SD), plotted against time.

(I) The same analysis as in (H) was carried out with the globin-TNF-α-CDE_{150} reporter.

(J) The effect of EGFP-Roquin overexpression on degradation of the control globin reporter mRNA lacking an insert as well as globin-TNF-α-CDE_{37}-V3 mRNA was examined by transient transfection in NIH 3T3 cells, as described in Figure 1E, average $t_{1/2} \pm$ SD, n = 3.

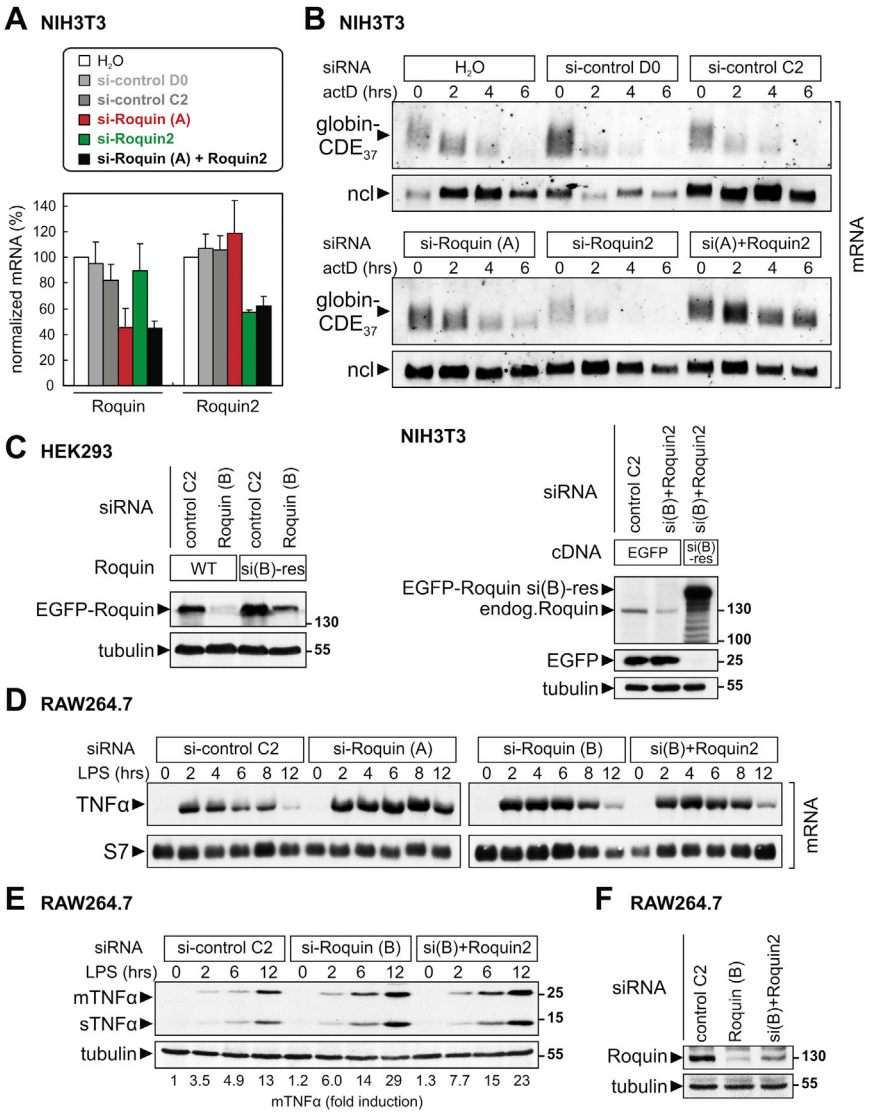

Figure S5. Knockdown of Roquin and Roquin2 Prevents CDE mRNA Degradation, Related to Figure 4

(A) For kd of Roquin and Roquin2, NIH 3T3 cells were transfected twice over a period of four days with either water (H_2O), control siRNAs (D0 or C2), or siRNAs against Roquin (A) or Roquin2, either alone or in combination. Roquin and Roquin2 mRNA levels were measured by RT-qPCR, normalized to ncl mRNA levels, and plotted as percentage of the water control (average ± SD, n ≥ 4).

(B) Roquin and Roquin2 were knocked down in NIH 3T3 cells is in (A). The globin-TNF-α-CDE_{37}-V3 reporter gene was included in the second transfection, and reporter mRNA decay was measured by northern blot analysis as described for Figure 1E. Quantification of n ≥ 3 repeat experiments is shown in Figure 4B.

(C) In the left panel, expression of EGFP-Roquin (WT) and the siRNA-resistant EGFP-Roquin si(B)-res was examined in HEK293 cells. The Roquin expressing plasmids were transfected together with the control siRNA C2 or the Roquin-siRNA (B). Cells were lysed after two days for western blot analysis using an anti-GFP antibody. In the right panel, EGFP or EGFP-Roquin-si(B)-res were transfected into NIH 3T3 cells one day after transfection of the control siRNA C2 or the Roquin-siRNA (B). Cells were lysed on day two and western blot analysis was carried out using an anti-Roquin antibody.

(D) TNF-α mRNA expression in response to LPS (100 ng/ml) was analyzed by northern blot in RAW264.7 cells transfected twice over a period of two days with control siRNA (C2), Roquin-siRNA (A), Roquin-siRNA (B) or Roquin-siRNA (B) together with Roquin2-siRNA.

(E) TNF-α production was analyzed in RAW264.7 cells transfected twice over a period of two days with control siRNA C2, Roquin-siRNA (B) or Roquin-siRNA (B) together with Roquin2-siRNA. Cells were stimulated with LPS (100 ng/ml), and total protein was extracted after 0, 2, 6 and 12 hr. Western blot analysis using an anti-TNF-α antibody shows membrane-bound (m)TNF-α and soluble (s)TNF-α. Quantification of mTNF-α normalized to tubulin is depicted below the blot. The first 8 lanes are the same as in Figure 4G, shown here again for comparison.

(F) Roquin expression was examined in protein lysates from cells shown in panel (E) by western blot analysis.

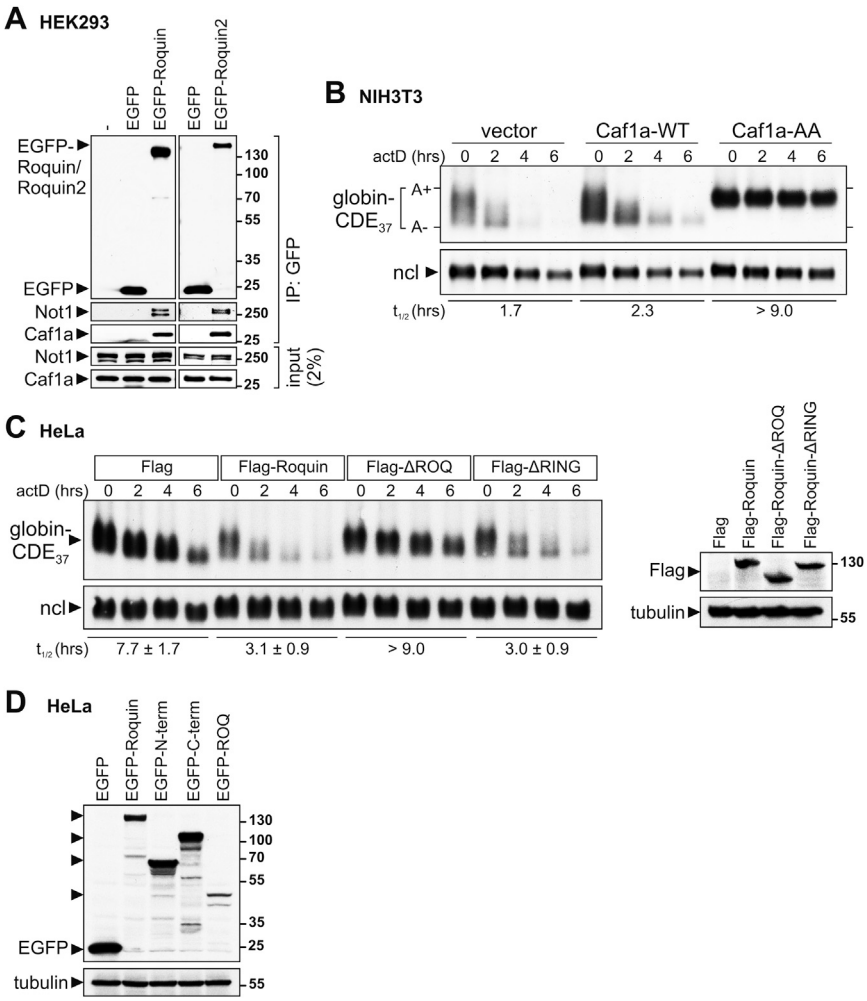

Figure S6. The CDE Induces Caf1-Dependent mRNA Deadenylation, Related to Figure 5

(A) HEK293 cells were transiently transfected with EGFP, EGFP-Roquin or EGFP-Roquin2. EGFP-tagged proteins were immunoprecipitated from cytoplasmic lysates, and endogenous Not1 as well as Caf1a were detected by western blot analysis. Depicted is a repeat experiment of the IP shown in Figure 5A to document specific association of Caf1a with EGFP-Roquin/Roquin2.

(B) NIH 3T3 cells were transiently transfected with globin-TNF-α-CDE_{37}-V3 together with either vector control, WT Caf1a or dominant-negative Caf1a-AA. mRNA degradation was analyzed as described for Figure 5B.

(C) Left: HeLa cells were transiently transfected with globin-TNF-α-CDE_{37}-V3 together with either Flag vector alone, Flag-Roquin, Flag-Roquin-ΔROQ or Flag-Roquin-ΔRING. Reporter mRNA degradation was analyzed as described in Figure 1E, average $t_{1/2} \pm$ SD, $n \geq 3$. Right: expression of Flag-Roquin, Flag-Roquin-ΔROQ and Flag-Roquin-ΔRING was examined by western blot analysis using an anti-Flag antibody.

(D) Expression of EGFP, EGFP-Roquin, EGFP-N-term, EGFP-C-term and EGFP-ROQ in transiently transfected HeLa cells was examined by western blot analysis using an anti-GFP antibody. This analysis corresponds to the experiment shown in Figure 5D.

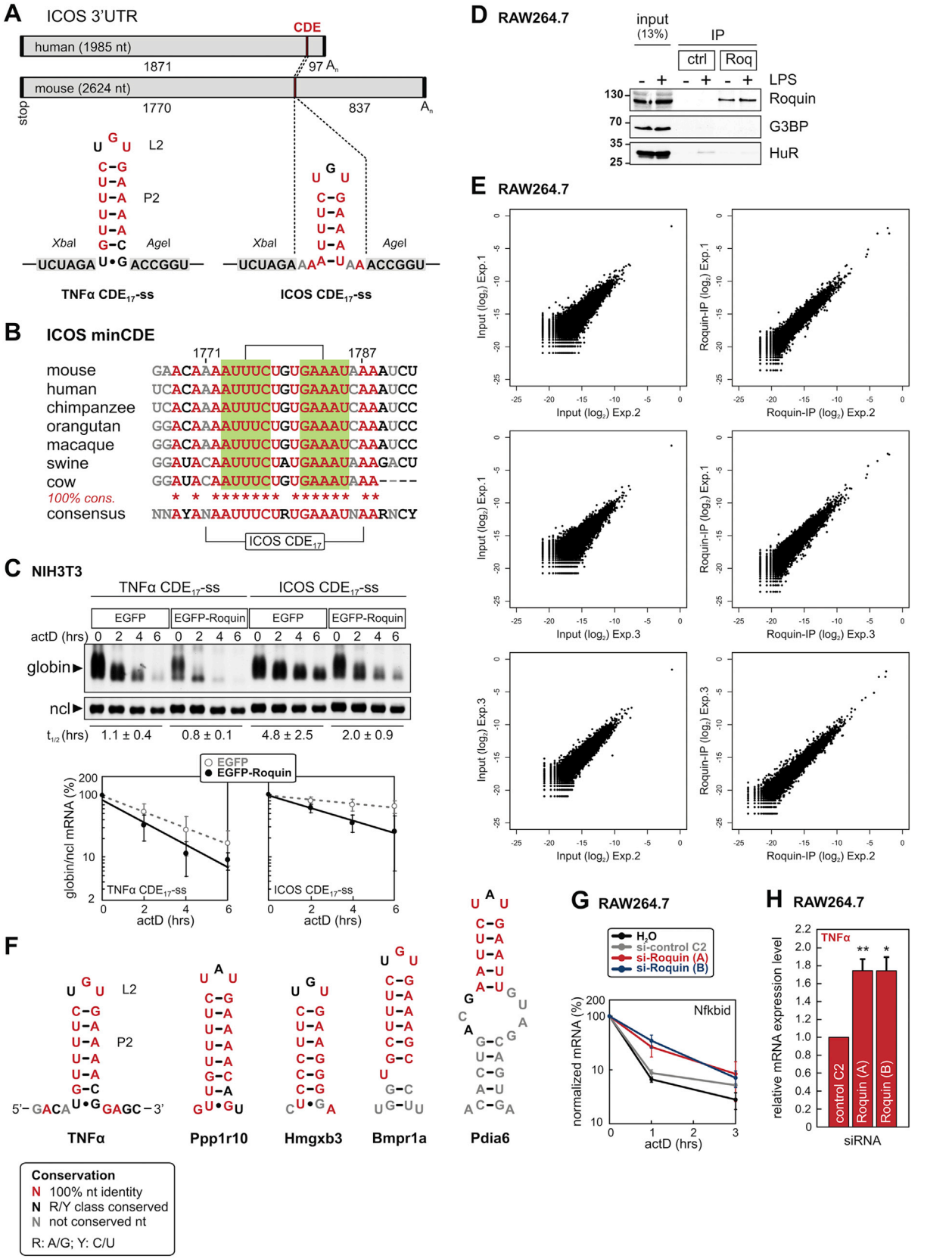

(legend on next page)

Figure S7. Genome-wide Identification of CDEs and Roquin Target mRNAs, Related to Figures 6 and 7

(A) Schematic representation of the human and mouse ICOS 3′UTRs. The CDE-like stem-loop in the mouse ICOS 3′UTR and, for comparison, the mouse TNF-α CDE_{17} are shown within the single-stranded (ss) cloning context. Nucleotides are color-coded according to conservation, as in Figure 1.

(B) Sequence conservation of the ICOS CDE based on the alignment of 7 mammalian species, numbers refer to nucleotide positions in the mouse ICOS 3′UTR. Nucleotides are color-coded according to conservation as in Figure 1, pairing elements are shaded in green.

(C) NIH 3T3 cells were transiently cotransfected with EGFP or EGFP-Roquin together with globin-TNF-α-CDE_{17}-ss or globin-ICOS-CDE_{17}-ss. Reporter mRNA decay was measured as in Figure 4A, average $t_{1/2} \pm$ SD, $n \geq 3$.

(D) Endogenous Roquin (Roq) was immunoprecipitated from cytoplasmic lysates of RAW264.7 macrophages ± stimulation with LPS (100 ng/ml) for 2 hr. HA-antibody was used for control (ctrl) IP. Roquin IP was monitored by western blot analysis, RNA-binding proteins G3BP and HuR serve as controls for specificity.

(E) Following IP of Roquin from LPS-stimulated RAW264.7 macrophages, mRNAs in the Roquin IP, control IP and input material were identified by RNA-Seq in three biological repeat experiments. To assess reproducibility, $\log_2$ of (read counts per gene / total read counts) in the Roquin IP and input samples was plotted as a pairwise comparison between the three experiments.

(F) Secondary structures were predicted for the CDEs of mouse Bmpr1a, Pdia6, Ppp1r10 and Hmgxb3, the TNF-α CDE is shown for comparison. Based on the UCSC genome alignment, nucleotides are color-coded according to conservation as in Figure 1D.

(G) Degradation of the tandem CDE-containing Nfkbid mRNA was measured by quantitative RT-qPCR in RAW264.7 macrophages after stimulation with LPS (100 ng/ml) for 2 hr. Nfkbid mRNA levels were normalized to NupL1 mRNA, average $t_{1/2} \pm$ SE, n = 3.

(H) RAW264.7 cells were transfected twice over a period of two days with control siRNA (C2) or two different siRNAs against Roquin (Roquin (A) and Roquin (B)). Cells were stimulated with LPS for 1 hr, and TNF-α mRNA levels were measured by RT-qPCR and normalized to NupL1 mRNA (average ± SE, n = 6). p values were calculated for Roquin (A) and Roquin (B) in comparison to control C2 by two-tailed, paired t test; ** indicates $p < 0.005$, *$p < 0.05$.